ΣNN quasibound states in ^{3}He$(K^-,\pi^\mp)$ reactions at 600 MeV/c

Toru Harada*
Research Center for Physics and Mathematics, Osaka Electro-Communication University, Neyagawa, Osaka, 572-8530, Japan and J-PARC Branch, KEK Theory Center, Institute of Particle and Nuclear Studies, High Energy Accelerator Research Organization (KEK), 203-1, Shirakata, Tokai, Ibaraki, 319-1106, Japan

Yoshiharu Hirabayashi
Information Initiative Center, Hokkaido University, Sapporo, 060-0811, Japan
(Received 18 February 2014; revised manuscript received 3 April 2014; published 7 May 2014)

We theoretically demonstrate the inclusive and semiexclusive spectra in the ^{3}He$(K^-,\pi^\mp)$ reactions at 600 MeV/c (4°) within a distorted-wave impulse approximation, using a coupled $(2N-\Lambda)+(2N-\Sigma)$ model with a spreading potential. We present the possible existence of the ΣNN quasibound state with $J^\pi = 1/2^+$, $T \simeq 1$ near the Σ threshold, predicted by a $2N-Y$ folding-model potential derived from YN g-matrices. The result shows that a signal of the $^3_\Sigma$He quasibound state is clearly confirmed near the Σ threshold in the π^- spectrum, whereas a peak of the $^3_\Sigma n$ quasibound state is rather reduced in the π^+ spectrum owing to the interference effects caused by the $^3S_1$-$^1S_0$ admixture in the NN pair. The mechanism of Σ production for these spectra and charge symmetry breaking effects are also discussed.

DOI: 10.1103/PhysRevC.89.054603 PACS number(s): 21.80.+a, 24.10.Eq, 25.80.Hp, 27.20.+n

I. INTRODUCTION

One of the most important subjects on strangeness nuclear physics is to understand properties of a Σ hyperon in nuclei as well as ΣN interaction [1]. The Σ hyperon is expected to play an essential role in the description of the ΛNN three-body force in hypernuclei [2], and the maximal mass and particle fraction of neutron stars or compact stars [3]. However, the ΣN interaction has still been in quantitative ambiguities because the ΣN scattering data are very limited [1,4].

In the 1990s, many efforts were made in Σ hypernuclear studies on s- and p-shell nuclei using $(K^-,\pi^\mp)$ reactions at CERN, BNL, and KEK [5,6]. It has been known that there is no evidence of a Σ nuclear state [7], except $^4_\Sigma$He which is established to be a quasibound (or unstable bound) state experimentally [8–10], as predicted in Ref. [11]. Saha *et al.* [12] reported that there is a strong repulsion in the real part with a sizable imaginary part of the Σ-nucleus potential analyzing nuclear (π^-,K^+) spectra on C, Si, Ni, In, and Bi targets. This repulsion originates from the ΣN $^3S_1$, $I=3/2$ channel that corresponds to a quark Pauli-forbidden state in baryon-baryon systems in the flavor SU(6) symmetry [13].

Several theoretical works [14–18] performed to investigate the ΣNN systems that have total isospin $T=0$, 1, 2 and total spin $S=1/2$, 3/2. Garcilazo [14] showed that the $\Sigma^- nn$ system with $T=2$ has no bound state in a Faddeev calculation with a separable ΣN potential, and Stadler and Gibson [15] confirmed it using the Jülich potential. Afnan and Gibson [16] demonstrated that an enhancement in the Λd cross section near the $\Sigma+N+N$ threshold is associated with a resonance pole of the ΣNN states having $T=0$, $S=1/2$ in the scattering amplitude. Dover *et al.* [17] discussed the spin-isospin selectivity of the $\Sigma N \to \Lambda N$ conversion decay in the ΣNN states, assuming that the isospin and spin of the NN pair, I_2 and S_2, are good quantum numbers. Their results suggested that the ΣNN state with $T=0$, $S=1/2$ is the best candidate to be bound and relatively long lived when the NN state takes $I_2=0$, $S_2=1$ [5]. It should be noticed that the NN states with $(I_2,S_2)=(1,0)$ and (0, 1) admix each other in the ΣNN state. Indeed, Koike and Harada [18] performed three-body ΣNN coupled-channel calculations, leading to the fact that there exist quasibound states of $T=1$, $S=1/2$ in the isotriplet ($^3_\Sigma$He, $^3_\Sigma$H, $^3_\Sigma n$) where the ΣN potential strongly admixes $(I_2,S_2)=(1,0)$ and (0, 1) states in the NN pair. Recently, Garcilazo *et al.* [19] have shown that a narrow quasibound state with $\Gamma \simeq 2.1$ MeV exists near the Σ threshold in the $T=1$, $S=1/2$ channel in ΣNN systems, using Faddeev ΛNN-ΣNN calculations with NN and YN potentials derived from a chiral constituent quark model. Consequently, one naively expects that the ΣNN quasibound state exists near the Σ threshold whenever a modern YN potential is used.

On the other hand, it has been recognized that there is no evidence of a narrow ΣNN quasibound state ($^3_\Sigma n$) below the Σ threshold in the ^{3}He(K^-,π^+) reaction at BNL-E774 experiments [20]. These contradictory arguments are still not settled: Is there a quasibound state in ΣNN systems?

In this paper, we theoretically demonstrate the inclusive and semiexclusive spectra in ^{3}He$(K^-,\pi^\mp)$ reactions at 600 MeV/c (4°) within a distorted-wave impulse approximation (DWIA), using a coupled $(2N-\Lambda)+(2N-\Sigma)$ model with a spreading potential. We focus on the behavior of signals of the ΣNN quasibound states observed as $^3_\Sigma$He and $^3_\Sigma n$ in π^- and π^+ spectra, respectively, in order to study the ΣN interaction and also a mechanism of Σ production for these spectra.

In a previous paper [21], we reported theoretical calculations of ^{3}He$(K^-,\pi^\mp)$ spectra at 600 MeV/c, using the $2N-Y$ folding-model potential with g-matrices derived from the NF$_S$ potential [22] that simulates the Nijmegen model F [23]. The result suggested that there are quasibound states in the ΣNN

*harada@isc.osakac.ac.jp

systems. However, the folding models using NF_S were not able to systematically explain Λ binding energies of ${}^{3}_{\Lambda}\mathrm{H}$, ${}^{4}_{\Lambda}\mathrm{He}$, ${}^{4}_{\Lambda}\mathrm{He}^*$, and ${}^{5}_{\Lambda}\mathrm{He}$. One of the prescriptions to solve this overbinding problem of s-shell Λ hypernuclei [24] may be to consider the coherent $\Lambda N - \Sigma N$ coupling [2]. The $D2$ potential [2,25] is a central version of the YN potential that simulates the Nijmegen model D [26], and it is fulfilled in the coherent $\Lambda N - \Sigma N$ coupling. In this paper, therefore, we use a slightly modified potential ($D2'$) that is adjusted to the binding energies of s-shell hypernuclei [27].

The outline of this paper is as follows. In Sec. II, we will briefly mention the DWIA framework for ${}^3\mathrm{He}(K^-,\pi^\mp)$ reactions, employing the coupled $(2N-\Lambda)+(2N-\Sigma)$ model in a Green's function technique [28,29]. In Sec. III, we will construct an effective $2N-Y$ potential within a microscopic folding model with YN g-matrices, and will discuss the structure of the ΣNN quasibound states, taking into account threshold effects due to the mass difference among Σ hyperons and the Coulomb forces. A pole position for the ΣNN quasibound state is obtained on the complex E plane. In Sec. IV, we will demonstrate the calculated spectra of the ${}^3\mathrm{He}(K^-,\pi^\mp)$ reactions at 600 MeV/c to see a possible signal of the ΣNN quasibound state, which might be observed in forthcoming experiments at J-PARC facilities [4]. In Sec. V, we will discuss the sensitivity of the $\pi^\mp$ spectra to a pole position of the ΣNN quasibound state. We will consider the reason why the peak of a ${}^{3}_{\Sigma}n$ quasibound state populated in the π^+ spectrum is not observed, and compare the calculated π^+ spectrum with the data observed in BNL-E774 experiments. Summary and conclusion are given in Sec. VI. In the Appendix, we will report binding energies of ${}^{3}_{\Lambda}\mathrm{H}$, ${}^{4}_{\Lambda}\mathrm{He}$, ${}^{4}_{\Lambda}\mathrm{He}^*$, and ${}^{5}_{\Lambda}\mathrm{He}$ obtained by the folding-model calculations with $D2'$, and interference effects for cross sections by $(K^-,\pi^\mp)$ reactions owing to the ${}^3S_1$-${}^1S_0$ admixture of the NN pair.

II. CALCULATIONS

Let us consider a theoretical framework for ${}^3\mathrm{He}(K^-,\pi^\mp)$ reactions. Here we treat hypernuclear final states classified as

$$\begin{aligned} K^{-}\,{}^3\mathrm{He} \to\ & \pi^- pp\Lambda,\\ & \pi^- d\Sigma^+,\\ & \pi^- pn\Sigma^+,\\ & \pi^- pp\Sigma^0, \end{aligned} \tag{1}$$

for the π^- spectrum, and those as

$$\begin{aligned} K^{-}\,{}^3\mathrm{He} \to\ & \pi^+ nn\Lambda,\\ & \pi^+ d\Sigma^-,\\ & \pi^+ pn\Sigma^-,\\ & \pi^+ nn\Sigma^0, \end{aligned} \tag{2}$$

for the π^+ spectrum. It seems that an impulse approximation works well in K^- capture at incident K^- beam of $p_{K^-} =$ 600 MeV/c [30]. Figure 1 illustrates typical diagrams for physical processes for the $(K^-,\ \pi^\mp)$ reactions. We will calculate these spectra within the distorted-wave impulse approximation (DWIA) for the $(2N-\Lambda)+(2N-\Sigma)$ model with a spreading potential [31], as we mention in this section.

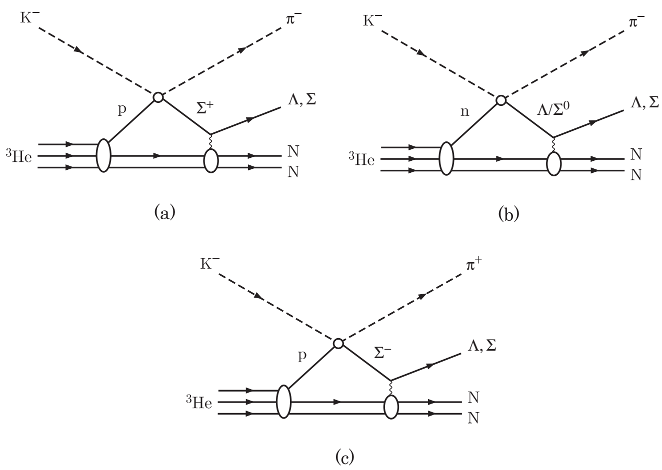

FIG. 1. Diagrams for hypernuclear $(K^-,\ \pi^\mp)$ reactions on a ${}^3\mathrm{He}$ target: (a) $K^- + p \to \pi^- + \Sigma^+$, (b) $K^- + n \to \pi^- + \Lambda$ or $K^- + n \to \pi^- + \Sigma^0$, and (c) $K^- + p \to \pi^+ + \Sigma^-$ reactions in the impulse approximation.

A. Model wave functions

In our calculation, we consider a model wave function Ψ_A of the ${}^3\mathrm{He}$ ground state ($J^\pi = 1/2^+, T = 1/2$) as a target nucleus, in the LS-coupling scheme. It is given by

$$\begin{aligned} |\Psi_A\rangle &= \hat{\mathcal{A}}\big[\big[\phi_0^{(2N)} \otimes \varphi_0^{(N)}\big]_{L_A} \otimes X^A_{T_A,S_A}\big]^{M_A}_{J_A},\\ X^A_{T_A,S_A} &= \big[\chi^{(2N)}_{I_2,S_2} \otimes \chi^{(N)}_{1/2,1/2}\big]_{1/2,1/2}, \end{aligned} \tag{3}$$

where $\hat{\mathcal{A}}$ is the antisymmetrized operator for nucleons, $\phi_0^{(2N)}$ is the wave function of a $2N$-core subsystem, and $\varphi_0^{(N)}$ is the relative wave function between $2N$ and N for a $2N-N$ system in the ${}^3\mathrm{He}$ ground state. $X^A_{T_A,S_A}$ is the isospin-spin function for ${}^3\mathrm{He}$, and $\chi^{(2N)}_{I_2,S_2}$ and $\chi^{(N)}_{1/2,1/2}$ are the isospin-spin functions for $2N$ (isospin I_2, spin S_2) and N ($I_N = 1/2, S_N = 1/2$), respectively. Here we obtain the wave function $\varphi_0^{(N)}$ using the $2N-N$ potential $U^{(N)}$ that was derived from microscopic three-body calculations [11] with a central potential of Tamagaki's C3G [32]. This potential can reproduce the experimental data of the binding energy of $B_N = 8.07$ MeV and the nuclear root-mean-square distance of $\langle R^2\rangle^{1/2} = 2.64$ fm for the ${}^2\mathrm{H} + p$ system in ${}^3\mathrm{He}$ [33].

For hypernuclear YNN final states, we consider wave functions Ψ_B for $2N-Y$ systems with J^π on physical particle (charge) bases. The wave functions are written by

$$\begin{aligned} |\Psi_B\rangle &= \sum_\alpha \big[\big[\phi_\alpha^{(2N)} \otimes \varphi^{(Y)}_{\ell_Y}\big]_{L_B} \otimes X^B_{Y_\alpha,S_\alpha}\big]^{M_B}_{J_B},\\ X^B_{Y_\alpha,S_\alpha} &= \big[\chi^{(2N)}_{I_2,S_2} \otimes \chi^{(Y)}_{I_Y,1/2}\big]_{Y_\alpha,S_\alpha}, \end{aligned} \tag{4}$$

where $\varphi^{(Y)}_{\ell_Y}$ is the relative wave function between $2N$ and Y with the angular momentum ℓ_Y, and $X^B_{Y_\alpha,S_\alpha}$ is the isospin-spin

TABLE I. Hypernuclear final states in $(K^-,\pi^\mp)$ reactions on a ^{3}He target and the threshold mass of the $2N-Y$ particle channels.

Reactions	Channels α	$M_{\rm th}$ (MeV)	$\omega_{\rm th}$ (MeV)	$\Delta M_{\rm th}$ (MeV)	I_2	S_2	S_α
(K^-,π^-)	$\{pp\}\Lambda$	2992.3	183.8	0.0	1	0	1/2
	$[pn]\Sigma^+$	3065.0	256.6	72.8	0	1	1/2, 3/2
	$\{pn\}\Sigma^+$	3067.2	258.8	75.0	1	0	1/2
	$\{pp\}\Sigma^0$	3069.2	260.8	77.0	1	0	1/2
(K^-,π^+)	$\{nn\}\Lambda$	2994.8	186.4	0.0	1	0	1/2
	$[pn]\Sigma^-$	3073.0	264.6	78.3	0	1	1/2, 3/2
	$\{pn\}\Sigma^-$	3075.2	266.8	80.5	1	0	1/2
	$\{nn\}\Sigma^0$	3071.6	263.2	77.0	1	0	1/2

function for $2N-Y$ in the α channel; $\chi^{(Y)}_{I_Y,1/2}$ is the isospin-spin function for Y (isospin I_Y, $S_Y=1/2$). The channel indices α indicate the final states as listed in Table I, where $\{N_1N_2\}=N_1N_2+N_2N_1$ and $[N_1N_2]=N_1N_2-N_2N_1$ denote the $2N$ states with $^1S_0$, $I=1$ and $^3S_1$, $I=0$, respectively. Since a spin-flip process in $(K^-,\pi^\mp)$ reactions at low momentum regions, e.g., $p_{K^-}=600$ MeV/c may be negligibly small, as seen in Sec. II E, we consider only spin $S_\alpha=1/2$ for the $2N-Y$ systems formed from ^{3}He, omitting $S_\alpha=3/2$. Therefore, we take the $2N-Y$ final states on $J_B=|L_B\pm 1/2|$ with $L_B=0,1,\dots,S_\alpha=1/2$, where J_B and L_B are the total and orbital angular momenta, respectively.

We use the wave functions $\phi^{(2N)}_\alpha$, which are obtained with the C3G potential. The wave function $\phi^{(2N)}_\alpha$ for the $[pn]$ ($^3S_1$, $I=0$) state has a nuclear bound state with $B_N=2.22$ MeV for ^{2}H($J^\pi=1^+$). Because there is no bound state in the $\{pp\}$ ($^1S_0$, $I=1$) state, we use a continuum-discretized wave function $\tilde\phi^{(2N)}_{\alpha,i}$ which is obtained in the momentum bin method [34],

$$\tilde\phi^{(2N)}_{\alpha,i}(\boldsymbol{r})=\frac{1}{\sqrt{\Delta k}}\int_{k_i}^{k_{i+1}}\phi^{(2N)}_\alpha(k,\boldsymbol{r})dk, \tag{5}$$

where $\Delta k=k_{i+1}-k_i$, and $\boldsymbol{r}$ and k are the radial coordinate and the momentum between two nucleons, respectively. The scattering wave function $\phi^{(2N)}_\alpha(k,\boldsymbol{r})$ satisfies the Schrödinger equation

$$\left(T_\alpha+v^{(NN)}_\alpha(\boldsymbol{r})-\varepsilon_\alpha\right)\phi^{(2N)}_\alpha(k,\boldsymbol{r})=0 \tag{6}$$

with the energy $\varepsilon_\alpha=k^2/2\mu$ (>0), where μ is the reduced mass of the $2N$ system. This method is often used in continuum-discretized coupled-channel (CDCC) calculations [34], and it may work well in continuum dynamics involving NN breakup processes. Here we used the only lowest discretized state with $k_0=0.0$ fm^{-1} and $\Delta k=0.20$ fm^{-1} for the $\{pp\}$ state.

Figure 2 shows the wave functions $\phi^{(2N)}_\alpha$ of the $[pn]$ and $\{pp\}$ states, together with the intranuclear $2N$ wave function $\phi^{(2N)}_0$ in the ^{3}He ground state, which is derived from three-body calculations with the C3G potential.

B. Distorted-wave impulse approximation

According to the DWIA [28,35–37], the inclusive differential cross section for nuclear (K^-,π) reactions in the laboratory frame is given by (in units $\hbar=c=1$)

$$\frac{d^2\sigma}{dE_\pi d\Omega_\pi}=\beta\frac{1}{[J_A]}\sum_{M_A}\sum_B|\langle\Psi_B|\hat F|\Psi_A\rangle|^2 \times\delta(E_\pi+E_B-E_K-E_A) \tag{7}$$

with the strangeness-exchange external operator including zero-range $K^-N\to\pi Y$ interactions

$$\hat F=\int d\boldsymbol{r}\,\chi^{(-)*}_\pi(\boldsymbol{p}_\pi,\boldsymbol{r})\chi^{(+)}_K(\boldsymbol{p}_K,\boldsymbol{r}) \times\sum_{j=1}^{A}\bar f_{(Y\pi)}(\omega_{\bar KN})\delta(\boldsymbol{r}-\boldsymbol{r}_j)\hat O_j, \tag{8}$$

where $[J]=2J+1$; E_π, E_K, E_B, and E_A are energies of an outgoing $\pi^\mp$, an incoming K^-, the hypernuclear state, and the target nucleus, respectively. The baryon operator $\hat O_j$ can change the jth nucleon into a hyperon in the nucleus, and $\boldsymbol{r}$ is the relative coordinate between the mesons and the center of mass of the nucleus; $\bar f_{(Y\pi)}$ is the Fermi-averaged amplitude for the $K^-+N\to\pi+Y$ reaction in the nuclear medium on the laboratory frame, where $\omega_{\bar KN}$ is the total energy of K^--N subsystems.

The momentum and energy transfer to the $2N-Y$ final state in these reactions is given by

$$\boldsymbol{q}=\boldsymbol{p}_K-\boldsymbol{p}_\pi,\quad \omega=E_K-E_\pi, \tag{9}$$

where $\boldsymbol{p}_K$ and $\boldsymbol{p}_\pi$ (E_K, E_π) are the laboratory momenta (energies) of the incident K^- and outgoing $\pi^\mp$ in the many-body $K^-+A\to\pi+{}^A_YB^*$ reaction, respectively. The kinematical factor β in Eq. (7) [38,39] expresses the translation from the two-body K^--N laboratory system to the K^--A

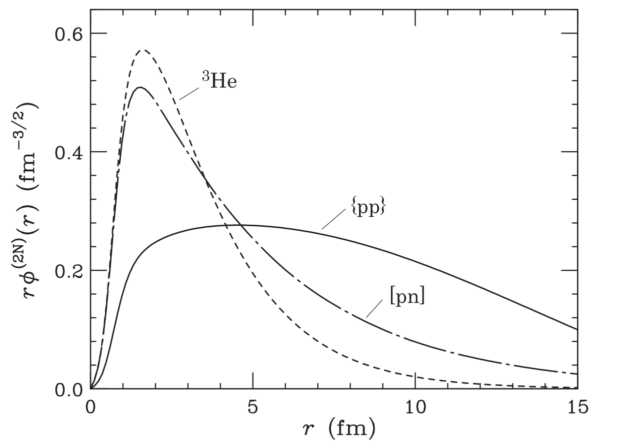

FIG. 2. Behaviors of the radial wave functions of the NN states, $r\phi^{(2N)}(r)$, as a function of the relative distance r between the nucleons. The solid and long-dashed-dot curves denote the wave functions for $\{pp\}$ and $[pn]$, respectively. The dashed curve denotes the intranuclear NN wave function in the ^{3}He ground state, which is obtained by three-body calculations. All of the wave functions are calculated with the central Tamagaki's C3G potential [32].

laboratory system [40], which is given by

$$\beta = \left(1 + \frac{E_\pi^{(0)}}{E_Y^{(0)}} \frac{p_\pi^{(0)} - p_K^{(0)} \cos\theta_{\rm lab}}{p_\pi^{(0)}}\right) \frac{p_\pi E_\pi}{p_\pi^{(0)} E_\pi^{(0)}}, \tag{10}$$

where $p_K^{(0)}$ and $p_\pi^{(0)}$ ($E_\pi^{(0)}$ and $E_Y^{(0)}$) are momenta of K^- and π (energies of π and hyperon) in the two-body $K^- + N \to \pi + Y$ reaction, respectively.

The distorted waves $\chi_\pi^{(-)*}$ and $\chi_K^{(+)}$ in Eq. (8) express the outgoing π and incoming K^- ones, respectively [41]:

$$\chi_\pi^{(-)*}(\boldsymbol{p}_\pi,\boldsymbol{r})\chi_K^{(+)}(\boldsymbol{p}_K,\boldsymbol{r}) = \sum_\lambda \sqrt{4\pi[\lambda]}\, i^\lambda \tilde{j}_\lambda(\theta_{\rm lab},r) Y_\lambda^0(\hat{\boldsymbol{r}}), \tag{11}$$

where $\tilde{j}_\lambda(\theta_{\rm lab},r)$ is the radial distorted wave with the angular momentum λ, and $\theta_{\rm lab}$ is the scattering angle to the forward direction in (K^-,π) reactions. The computational procedure for the distorted waves is simplified with the help of the eikonal approximation [35,42] because the distortions for mesons are not so important in few-body systems.

According to the Green's function method [28,29], we can rewrite a sum of the final states in Eq. (7) as

$$\sum_B |\Psi_B\rangle\langle\Psi_B|\delta(E - E_B) = -\frac{1}{\pi}{\rm Im}\hat{G}(E). \tag{12}$$

Thus the inclusive differential cross section is written by

$$\frac{d^2\sigma}{dE_\pi d\Omega_\pi} = \beta \frac{1}{[J_A]} \sum_{M_A} S_\pi, \tag{13}$$

where the strength function is given by

$$S_\pi = -\frac{1}{\pi}{\rm Im}\langle F|\hat{G}(E)|F\rangle, \tag{14}$$

where $|F\rangle$ denotes the $2N - Y$ doorway states excited initially by external field, which is defined as

$$|F\rangle \equiv \hat{F}|\Psi_A\rangle, \tag{15}$$

involving the $\overline{f}_{(Y\pi)}$ amplitudes.

C. Coupled-channel Green's functions

The Green's function method [28,29] facilitates parametrizing complicated many-body effects in a simple and tractable way, keeping the proper aspects of quantum mechanical systems. This technique can well describe an unstable hadron nuclear system such as a Σ^-, Ξ^-, or K^- nuclear state [29]. The complete Green's function G in Eq. (14) [43] provides all information concerning hyperon-nucleus dynamics as a function of the energy transfer $\omega = E_B - E_A$, which is related to the energy $E_Y = E_B - (m_Y + M_C) = -B_Y$ measured from the Y+core-nucleus threshold, where m_Y and M_C are masses of the Y and the core nucleus, respectively. Here we will consider $2N - Y$ states within coupled $(2N - \Lambda) + (2N - \Sigma)$ channels with a spreading potential [30].

For $2N - Y$ final states, the complete Green's function in the P space is given by

$$\hat{G}(\omega) = P \frac{1}{\omega - \hat{H} + i\epsilon} P, \tag{16}$$

where $\hat{H}$ is the total Hamiltonian of the $2N - Y$ system with $\hat{H}|\Psi_B\rangle = E_B|\Psi_B\rangle$, and P is Feshbach's projection operator for the model space we consider. Then we can calculate the complete Green's function by solving the following equation:

$$\hat{G}(\omega) = \hat{G}^{(0)}(\omega) + \hat{G}^{(0)}(\omega)\hat{U}\hat{G}(\omega), \tag{17}$$

where $\hat{G}^{(0)}$ is the free Green's function for the $2N - Y$ system, and $\hat{U}$ is the operator of a potential energy for the relative motion between $2N$ and Y. In order to extend it to a coupled-channel system, we introduce projection operators of P_α into the α channel in the P space, where $P = \sum_\alpha P_\alpha$. In the case of $P = P_\alpha + P_{\alpha'}$, for example, we obtain

$$\begin{aligned}\hat{G}(\omega) &= (P_\alpha + P_{\alpha'})\hat{G}(\omega)(P_\alpha + P_{\alpha'})\\ &= \hat{G}_{\alpha\alpha}(\omega) + \hat{G}_{\alpha\alpha'}(\omega) + \hat{G}_{\alpha'\alpha}(\omega) + \hat{G}_{\alpha'\alpha'}(\omega),\end{aligned} \tag{18}$$

where we define $\hat{G}_{\alpha\alpha'}(\omega) = P_\alpha\hat{G}(\omega)P_{\alpha'}$. The complete Green's function for $\alpha\alpha'$ channels satisfies the following multichannel coupled equation:

$$\hat{G}_{\alpha\alpha'}(\omega) = \hat{G}_\alpha^{(0)}(\omega)\delta_{\alpha\alpha'} + \hat{G}_\alpha^{(0)}(\omega)\sum_\gamma \hat{U}_{\alpha\gamma}\hat{G}_{\gamma\alpha'}(\omega). \tag{19}$$

Solving this coupled equation numerically, we obtain the complete Green's function $\hat{G}_{\alpha\alpha'}(\omega)$ [44]. Here we use partial waves of $\hat{G}_{\alpha\alpha'}(\omega)$ with J_B as a function of the relative distance R between $2N$ and Y, and its explicit form is written as

$$\begin{aligned}&G^{J_B}_{Y\alpha Y'\alpha'}(\omega;\boldsymbol{R},\boldsymbol{R}')\\ &\quad = \sum_{LM} \Phi^{(LS)J_BM_B}_{Y\alpha}(\hat{\boldsymbol{R}})\big|\phi_\alpha^{(2N)}\big\rangle \frac{g^{(\alpha\alpha')J_B}_{YY'}(\omega;R,R')}{RR'}\\ &\qquad \times\big\langle\phi_{\alpha'}^{(2N)}\big|\Phi^{(LS)J_BM_B}_{Y'\alpha'}(\hat{\boldsymbol{R}}')^\dagger\end{aligned} \tag{20}$$

with

$$\Phi^{(LS)J_BM_B}_{Y\alpha}(\hat{\boldsymbol{R}}) = \big[Y_{L_B}(\hat{\boldsymbol{R}}) \otimes X^B_{Y_\alpha,S_\alpha}\big]^{J_BM_B}_{Y\alpha}, \tag{21}$$

where $g^{(\alpha\alpha')J}_{YY'}(\omega;R,R')$ is the relative Green's function for $Y\alpha Y'\alpha'$ channels. The explicit form of the double-differential cross section of Eq. (13) is written as

$$\begin{aligned}\frac{d^2\sigma}{d\Omega_\pi dE_\pi} &= \sum_{J\lambda\alpha\alpha'YY'} \overline{f}^*_{(Y\pi)}\overline{f}_{(Y'\pi)}C^*_{Y\alpha}C_{Y'\alpha'}\\ &\quad\times\big\langle\phi_\alpha^{(2N)}\big|\phi_0^{(2N)}\big\rangle^*\big\langle\phi_{\alpha'}^{(2N)}\big|\phi_0^{(2N)}\big\rangle(-)^{S'+S+2J_A}\\ &\quad\times[J_B][\lambda]\sqrt{[L_A][L_B][L'_A][L'_B]}\, I^{(\alpha\alpha')J_B}_{YY'NN'}(\theta_{\rm lab},\omega)\\ &\quad\times\begin{pmatrix} L_B & \lambda & L_A\\ 0 & 0 & 0\end{pmatrix}\begin{Bmatrix} J_B & \lambda & J_A\\ L_A & S & L_B\end{Bmatrix}\\ &\quad\times\begin{pmatrix} L'_B & \lambda & L'_A\\ 0 & 0 & 0\end{pmatrix}\begin{Bmatrix} J_B & \lambda & J_A\\ L_{A'} & S' & L_{B'}\end{Bmatrix}\end{aligned} \tag{22}$$

with

$$\begin{aligned}I^{(\alpha\alpha')J_B}_{YY'NN'}(\theta_{\rm lab},\omega) &= (-)\frac{1}{\pi}{\rm Im}\int_0^\infty dRdR'RR'\varphi_0^{(N)}(R)\\ &\quad\times\tilde{j}_\lambda^{(+)*}\left(\theta_{\rm lab},\frac{M_C}{M_A}R\right)g^{(\alpha\alpha')J_B}_{YY'}(\omega;R,R')\\ &\quad\times\tilde{j}_\lambda^{(+)}\left(\theta_{\rm lab},\frac{M_C}{M_A}R'\right)\varphi_0^{(N)}(R'),\end{aligned} \tag{23}$$

TABLE II. Isospin-spin spectroscopic factor $C_{Y\alpha}$ for the $2N$–Y channel.

Reactions	Channels	$C_{Y\alpha}$
(K^-,π^-)	$\{pp\}\Lambda$	-1
	$[pn]\Sigma^+$	$\sqrt{3/2}$
	$\{pn\}\Sigma^+$	$\sqrt{1/2}$
	$\{pp\}\Sigma^0$	-1
(K^-,π^+)	$\{nn\}\Lambda$	-1
	$[pn]\Sigma^-$	$\sqrt{3/2}$
	$\{pn\}\Sigma^-$	$\sqrt{1/2}$
	$\{nn\}\Sigma^0$	-1

where the factor of M_C/M_A denotes the recoil effects, leading to the effective momentum transfer of $(M_C/M_A)q$. The isospin-spin spectroscopic factor for the $2N-Y$ channel is obtained as

$$C_{Y\alpha} = \langle X^B_{Y,S}|\sum_{j=1}^{A}\hat{O}_j|X^A_{T_A,S}\rangle. \tag{24}$$

In Table II, we show the values of $C_{Y\alpha}$ for non-spin-flip processes, which are seemed to be dominant ones in nuclear (K^-,π) reactions near 600 MeV/c.

D. The decomposition of the inclusive cross sections into components

The inclusive cross sections can be decomposed into partial cross sections corresponding to different physical processes [28,29,45], as classified in Table I. We obtain the decomposition of the strength function S_π of Eq. (14) as

$$S_{\pi^-} = S^{\{pp\}\Lambda}_{\pi^-} + S^{[pn]\Sigma^+}_{\pi^-} + S^{\{pn\}\Sigma^+}_{\pi^-} + S^{\{pp\}\Sigma^0}_{\pi^-} + S^{(\mathrm{Conv})}_{\pi^-} \tag{25}$$

for the π^- spectrum, and that as

$$S_{\pi^+} = S^{[pn]\Sigma^-}_{\pi^+} + S^{\{pn\}\Sigma^-}_{\pi^+} + S^{\{nn\}\Sigma^0}_{\pi^+} + S^{(\mathrm{Conv})}_{\pi^+} \tag{26}$$

for the π^+ spectrum. The partial strength functions are defined by

$$\begin{aligned} S^\alpha_\pi &= -\frac{1}{\pi}\langle F|\hat{\Omega}^{(-)\dagger}\big(\mathrm{Im}\hat{G}^{(0)}_\alpha\big)\hat{\Omega}^{(-)}|F\rangle,\\ S^{(\mathrm{Conv})}_\pi &= -\frac{1}{\pi}\sum_{\alpha\alpha'}\langle F|\hat{G}^\dagger_\alpha W_{\alpha\alpha'}\hat{G}_{\alpha'}|F\rangle, \end{aligned} \tag{27}$$

where we used the identity

$$\mathrm{Im}\hat{G} = \hat{\Omega}^{(-)\dagger}(\mathrm{Im}\hat{G}^{(0)})\hat{\Omega}^{(-)} + \hat{G}^\dagger(\mathrm{Im}\hat{U})\hat{G}, \tag{28}$$

and $\hat{\Omega}^{(-)} = 1 + \hat{U}\hat{G}$ is the Möller wave operator, and $W_{\alpha\alpha'}$ is a *spreading* (imaginary) potential for the complicated nuclear excited states from the $\alpha\alpha'$ channel. It should be noticed that $\hat{G}^\dagger_\alpha W_{\alpha\alpha'}\hat{G}_{\alpha'}$ denotes the spreading processes, which are predominantly caused by the $\Sigma N \to \Lambda N$ conversion into complicated $N+N+\Lambda$ states because a produced Σ subsequently interacts with a second nucleon, and its converted ΛN pair gains large energy from the mass difference $m_\Sigma - m_\Lambda \simeq$ 70 MeV. Indeed, the peak below the Σ threshold is connected with the secondary processes

$$\left[{}^3_\Sigma\mathrm{He}\right] \to p + p + \Lambda, \tag{29}$$

in the π^- spectrum, or with those

$$\left[{}^3_\Sigma n\right] \to n + n + \Lambda, \tag{30}$$

in the π^+ spectrum. The decomposition near the Σ threshold can help us to understand the structure of the YNN quasibound state and its decay property.

E. Fermi-averaged amplitudes for $K^- + N \to \pi + Y$ in nuclear medium

It is recognized that the spectral shape for DWIA is sensitive to the elementary $K^- + N \to \pi + Y$ amplitudes of $\overline{f}_{(Y\pi)}$ in nuclear medium in Eq. (8) [37,46–48]. When we evaluate the nuclear $(K^-,\pi^\mp)$ cross sections with the $K^- + N \to \pi + Y$ amplitudes, it is important to take into account the Fermi motion of a struck nucleon in nuclear medium [37]. This effect is considerably enhanced near narrow Λ/Σ resonances because their widths are smaller than the Fermi-motion energy of the struck nucleon. According to the procedure by Rosenthal and Tabakin [46], we perform the Fermi-averaging of the $K^- + N \to \pi + Y$ scattering T matrix obtained by Gopal *et al.* [49]. We use the momentum distribution $\rho(p)$ of a struck nucleon in ^{3}He, which is assumed as a simple harmonic oscillator with a size parameter $b_N = 1.31$ fm, leading to $\langle p^2\rangle^{1/2} \simeq 184$ MeV/c in the nucleus.

In Fig. 3, we show the Fermi-averaged laboratory cross sections of $K^- + n \to \pi^- + \Lambda$, $K^- + p \to \pi^- + \Sigma^+$, $K^- + n \to \pi^- + \Sigma^0$, and $K^- + p \to \pi^+ + \Sigma^-$ reactions on nuclei,

$$\left\langle\frac{d\sigma}{d\Omega}\right\rangle^{K^-N\to\pi Y}_{\mathrm{lab}} = |\overline{f}_{(Y\pi)}|^2 + |\overline{g}_{(Y\pi)}|^2, \tag{31}$$

at detected π angles $\theta_{\mathrm{lab}} = 0^\circ$ and 10°, as a function of the incident K^- laboratory momentum p_K. $\overline{f}_{(Y\pi)}$ and $\overline{g}_{(Y\pi)}$ denote the non-spin-flip and spin-flip components of the Fermi-averaged amplitudes, respectively. The shape of the Fermi-averaged cross section sizably becomes broader, and its value is not so changed by a choice of the target, as discussed by Dover *et al.* [5,42,48]. Since the spin-flip cross section of $|\overline{g}_{(Y\pi)}|^2$ is negligibly small, we consider only the non-spin-flip process in the nuclear $(K^-,\pi^\mp)$ reaction.

Furthermore, it is noticed that the Fermi-averaged amplitudes $\bar{f}_{(Y\pi)}$ remain in ambiguities, e.g., the relative phase of φ_Λ (φ_Σ) for $\Lambda\pi$ ($\Sigma\pi$ $I=1$) to $\Sigma\pi$ $I=0$ channels, as discussed in Ref. [30]. Thus we assume $\varphi_\Lambda = +15.8^\circ$ and $\varphi_\Sigma = +33.2^\circ$, which were determined by fitting the data overall in ^{4}He$(K^-,\pi^\mp)$ reactions at $p_{K^-} = 600$ MeV/c [30], and we use them in our calculations.

III. MICROSCOPIC COUPLED-CHANNEL $2N-Y$ POTENTIALS

In order to describe the ΣNN quasibound states, we construct a microscopic effective $2N-Y$ potential using the YN g-matrices in folding-model calculations [52,58]. In Ref. [18], three-body coupled-channel calculations for ΣNN

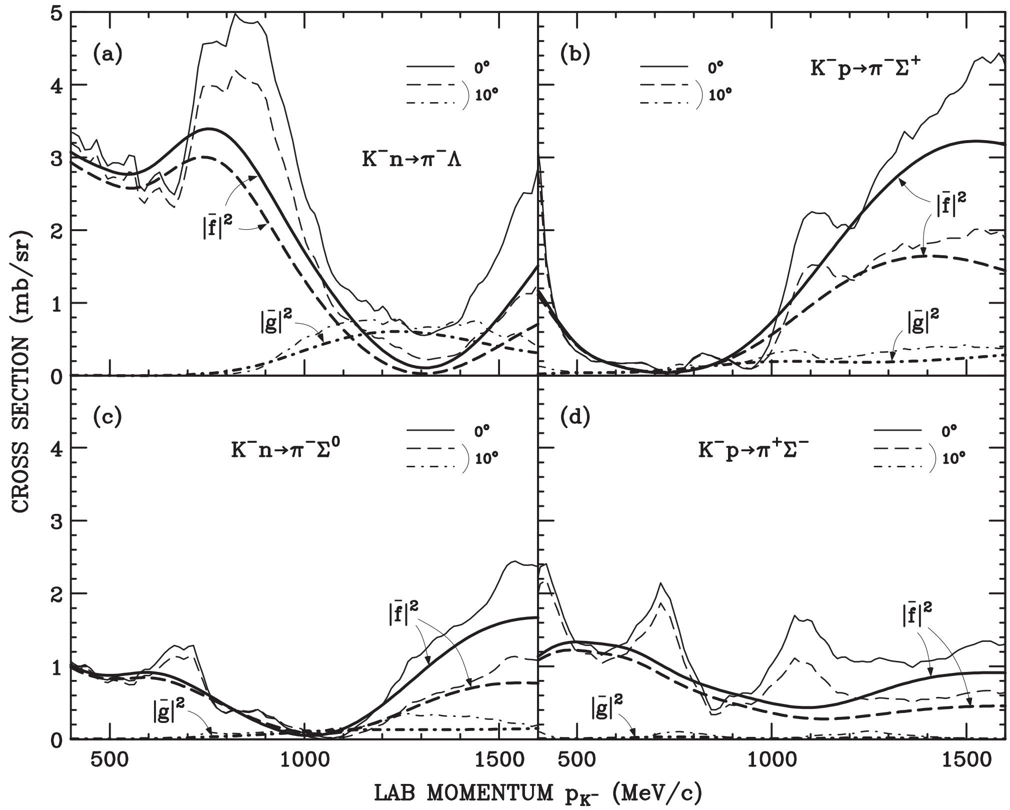

FIG. 3. Fermi-averaged cross sections for (a) $K^- + n \to \pi^- + \Lambda$, (b) $K^- + p \to \pi^- + \Sigma^+$, (c) $K^- + n \to \pi^- + \Sigma^0$, and (d) $K^- + p \to \pi^+ + \Sigma^-$ reactions in nuclear medium. Solid and long-dashed curves denote non-spin-flip Fermi-averaged laboratory cross sections, $|\overline{f}|^2$, for $\theta_{\rm lab} = 0^\circ$ and 10°, respectively, and the dot-dashed curve denotes a spin-flip Fermi-averaged one, $|\overline{g}|^2$, for $\theta_{\rm lab} = 10^\circ$. The thin-solid and thin-dashed curves are for non-spin-flip laboratory elementary cross sections in free space at $\theta_{\rm lab} = 0^\circ$ and 10°, respectively, and the thin-dot-dashed curve is for a spin-flip one at $\theta_{\rm lab} = 10^\circ$. The elementary amplitudes are used by Gopal *et al.* [49].

systems suggested that the channel coupling plays an important role in making a bound state which has strong admixtures of $(I_2,S_2) = (0,\ 1)$ and $(1,\ 0)$ states in the NN pair, e.g., $[pn]\Sigma^+$, $\{pn\}\Sigma^+$, and $\{pp\}\Sigma^0$ states admix each other in ${}^3_\Sigma$He. Its origin is due to the $(\boldsymbol{\sigma}_N \cdot \boldsymbol{\sigma}_\Sigma)(\boldsymbol{\tau}_N \cdot \boldsymbol{t}_\Sigma)$ term in the ΣN OBE potentials [5]. This nature is quite different from the weak-coupling state like $[pn] + \Lambda$ in ${}^3_\Lambda$H, and it must be involved in the $2N - Y$ potential.

In folding-model calculations, the effective $2N - Y$ potential for $\alpha\alpha'$ channels is obtained as

$$U_{\alpha\alpha'}(\boldsymbol{R}) = \int \rho_{\alpha\alpha'}(\boldsymbol{r})(\overline{g}_{\alpha\alpha'}(\boldsymbol{r}_1) + \overline{g}_{\alpha\alpha'}(\boldsymbol{r}_2))d\boldsymbol{r}, \qquad (32)$$

where $\boldsymbol{r}_1 = \boldsymbol{R} + \boldsymbol{r}/2\,(\boldsymbol{r}_2 = \boldsymbol{R} - \boldsymbol{r}/2)$ is the relative coordinate between N_1 (N_2) and Y, as shown in Fig. 4. The nucleon or transition density for $\alpha\alpha'$ channels is given by

$$\rho_{\alpha\alpha'}(\boldsymbol{r}) = \big\langle \phi_\alpha^{(2N)} \big| \sum_i \delta(\boldsymbol{r} - \boldsymbol{r}_i) \big| \phi_{\alpha'}^{(2N)} \big\rangle. \qquad (33)$$

In Table III, we show matrix elements of isospin-spin averaged potentials for $\alpha\alpha'$ channels, in which the g-matrices $\overline{g}_{\alpha\alpha'}$ for $\Lambda N - \Lambda N$, $\Lambda N - \Sigma N$, and $\Sigma N - \Sigma N$ states can be obtained by solving the coupled Bethe-Goldstone equation with appropriate parameters of the starting energy E_S and Fermi momentum $k_{\rm F}$.

Figure 5 shows the wave functions for $\rho_{\alpha\alpha'}$ of Eq. (33), as a function of the distance r between nucleons. For the $\{pp\}\Lambda$ channel, here we used the $\{pp\}$ wave function $\phi_\alpha^{(2N)}$ obtained by CDCC as the NN-pair nucleus, as given in Fig. 2, because the ΛN interaction is very weak. For the Σ channels, on the other hand, we must consider nuclear contraction of the NN pair because ΣN potentials may induce NN-pair admixture between ${}^3S_1$ and ${}^1S_0$ states in ΣNN systems [18]. In the $[pn]\Sigma^+$ channel, the wave function derived from three-body ΣNN calculations is not so changed that in ^{2}H. In the $\{pp\}\Sigma^0$ or

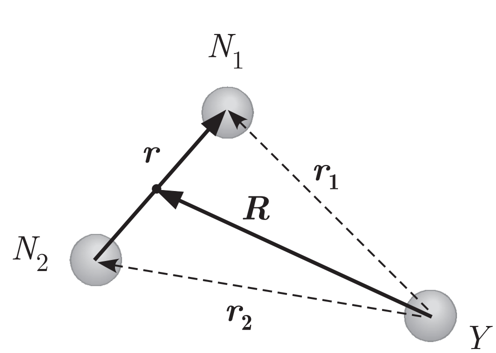

FIG. 4. Coordinates of the $2N - Y$ systems when calculating the effective $2N - Y$ potentials.

TABLE III. Isospin-spin averaged matrix elements of $\overline{g}_{\alpha\alpha'}$ for the YN potential terms in ${}^3_Y$He and ${}^3_Y n$. $g^{YY'}_{I,S}$ denotes a $YN - Y'N$ potential for the isospin I and spin S state.

α	α'	$\overline{g}_{\alpha\alpha'}$
$\{pp\}\Lambda$	$\{pp\}\Lambda$	$+\frac{3}{4}g^{\Lambda\Lambda}_{1/2,1} + \frac{1}{4}g^{\Lambda\Lambda}_{1/2,0}$
	$[pn]\Sigma^+$	$-\frac{3}{4}g^{\Lambda\Sigma}_{1/2,1} + \frac{1}{4}g^{\Lambda\Sigma}_{1/2,0}$
	$\{pn\}\Sigma^+$	$-\sqrt{\frac{1}{3}}\left(\frac{3}{4}g^{\Lambda\Sigma}_{1/2,1} + \frac{1}{4}g^{\Lambda\Sigma}_{1/2,0}\right)$
	$\{pp\}\Sigma^0$	$+\sqrt{\frac{1}{3}}\left(\frac{3}{4}g^{\Lambda\Sigma}_{1/2,1} + \frac{1}{4}g^{\Lambda\Sigma}_{1/2,0}\right)$
$[pn]\Sigma^+$	$[pn]\Sigma^+$	$\frac{2}{12}g^{\Sigma\Sigma}_{3/2,1} + \frac{6}{12}g^{\Sigma\Sigma}_{3/2,0} + \frac{1}{12}g^{\Sigma\Sigma}_{1/2,1} + \frac{3}{12}g^{\Sigma\Sigma}_{1/2,0}$
	$\{pn\}\Sigma^+$	$-\frac{\sqrt{3}}{12}\left(g^{\Sigma\Sigma}_{3/2,1} - g^{\Sigma\Sigma}_{3/2,0} - g^{\Sigma\Sigma}_{1/2,1} + g^{\Sigma\Sigma}_{1/2,0}\right)$
	$\{pp\}\Sigma^0$	$+\frac{\sqrt{3}}{12}\left(g^{\Sigma\Sigma}_{3/2,1} - g^{\Sigma\Sigma}_{3/2,0} - g^{\Sigma\Sigma}_{1/2,1} + g^{\Sigma\Sigma}_{1/2,0}\right)$
$\{pn\}\Sigma^+$	$\{pn\}\Sigma^+$	$\frac{6}{12}g^{\Sigma\Sigma}_{3/2,1} + \frac{2}{12}g^{\Sigma\Sigma}_{3/2,0} + \frac{3}{12}g^{\Sigma\Sigma}_{1/2,1} + \frac{1}{12}g^{\Sigma\Sigma}_{1/2,0}$
	$\{pp\}\Sigma^0$	$\frac{3}{12}g^{\Sigma\Sigma}_{3/2,1} + \frac{1}{12}g^{\Sigma\Sigma}_{3/2,0} - \frac{3}{12}g^{\Sigma\Sigma}_{1/2,1} - \frac{1}{12}g^{\Sigma\Sigma}_{1/2,0}$
$\{pp\}\Sigma^0$	$\{pp\}\Sigma^0$	$\frac{6}{12}g^{\Sigma\Sigma}_{3/2,1} + \frac{2}{12}g^{\Sigma\Sigma}_{3/2,0} + \frac{3}{12}g^{\Sigma\Sigma}_{1/2,1} + \frac{1}{12}g^{\Sigma\Sigma}_{1/2,0}$
$\{nn\}\Lambda$	$\{nn\}\Lambda$	$+\frac{3}{4}g^{\Lambda\Lambda}_{1/2,1} + \frac{1}{4}g^{\Lambda\Lambda}_{1/2,0}$
	$[pn]\Sigma^-$	$-\frac{3}{4}g^{\Lambda\Sigma}_{1/2,1} + \frac{1}{4}g^{\Lambda\Sigma}_{1/2,0}$
	$\{pn\}\Sigma^-$	$+\sqrt{\frac{1}{3}}\left(\frac{3}{4}g^{\Lambda\Sigma}_{1/2,1} + \frac{1}{4}g^{\Lambda\Sigma}_{1/2,0}\right)$
	$\{nn\}\Sigma^0$	$-\sqrt{\frac{1}{3}}\left(\frac{3}{4}g^{\Lambda\Sigma}_{1/2,1} + \frac{1}{4}g^{\Lambda\Sigma}_{1/2,0}\right)$
$[pn]\Sigma^-$	$[pn]\Sigma^-$	$\frac{2}{12}g^{\Sigma\Sigma}_{3/2,1} + \frac{6}{12}g^{\Sigma\Sigma}_{3/2,0} + \frac{1}{12}g^{\Sigma\Sigma}_{1/2,1} + \frac{3}{12}g^{\Sigma\Sigma}_{1/2,0}$
	$\{pn\}\Sigma^-$	$+\frac{\sqrt{3}}{12}\left(g^{\Sigma\Sigma}_{3/2,1} - g^{\Sigma\Sigma}_{3/2,0} - g^{\Sigma\Sigma}_{1/2,1} + g^{\Sigma\Sigma}_{1/2,0}\right)$
	$\{nn\}\Sigma^0$	$-\frac{\sqrt{3}}{12}\left(g^{\Sigma\Sigma}_{3/2,1} - g^{\Sigma\Sigma}_{3/2,0} - g^{\Sigma\Sigma}_{1/2,1} + g^{\Sigma\Sigma}_{1/2,0}\right)$
$\{pn\}\Sigma^-$	$\{pn\}\Sigma^-$	$\frac{6}{12}g^{\Sigma\Sigma}_{3/2,1} + \frac{2}{12}g^{\Sigma\Sigma}_{3/2,0} + \frac{3}{12}g^{\Sigma\Sigma}_{1/2,1} + \frac{1}{12}g^{\Sigma\Sigma}_{1/2,0}$
	$\{nn\}\Sigma^0$	$\frac{3}{12}g^{\Sigma\Sigma}_{3/2,1} + \frac{1}{12}g^{\Sigma\Sigma}_{3/2,0} - \frac{3}{12}g^{\Sigma\Sigma}_{1/2,1} - \frac{1}{12}g^{\Sigma\Sigma}_{1/2,0}$
$\{nn\}\Sigma^0$	$\{nn\}\Sigma^0$	$\frac{6}{12}g^{\Sigma\Sigma}_{3/2,1} + \frac{2}{12}g^{\Sigma\Sigma}_{3/2,0} + \frac{3}{12}g^{\Sigma\Sigma}_{1/2,1} + \frac{1}{12}g^{\Sigma\Sigma}_{1/2,0}$

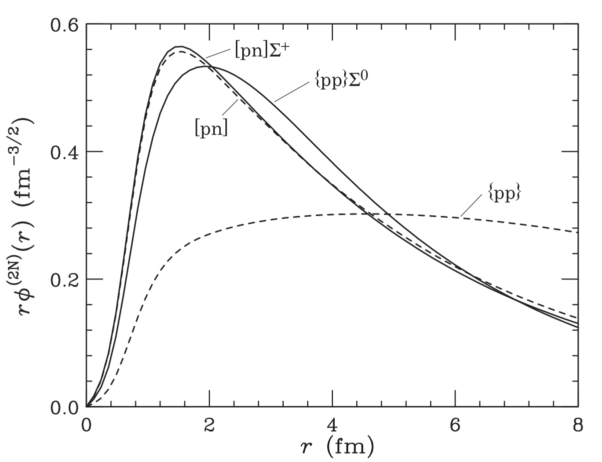

FIG. 5. Radial wave functions of the intranuclear NN states in transition densities of $\rho_{\alpha\alpha'}$, which are used to calculate the $2N - Y$ potentials in the folding model, as a function of the relative distance r. The solid curve denote the NN wave functions in the ΣNN quasibound state, which is obtained by three-body calculations [18]. The dash curves denote the NN wave functions in free space.

$\{pn\}\Sigma^+$ channel, the wave functions in the ΣNN systems differ from that obtained by CDCC, and the root-mean-square radius amounts to $\langle r^2\rangle^{1/2} = 3.7$ fm for the former, in a comparison with 7.7 fm for the latter. This contraction makes a strong coupling between the $\{pn\}\Sigma^+$, $[pn]\Sigma^+$, and $\{pp\}\Sigma^0$ states in ${}^3_\Sigma$He, leading to the results that will confirm the structure of ΣNN quasibound states obtained in three-body calculations [18]. In folding-model calculations, therefore, we use these wave functions derived from three-body ΣNN calculations.

Now let us calculate the YN g-matrices in Eq. (32) with a central version ($D2'$) of the YN potential [2,22] that simulates the Nijmegen model D [23]. This $D2'$ potential has the ability of solving the overbinding problem of Λ-binding energies of s-shell Λ hypernuclei in Brueckner-Hartree-Fock [2] and full few-body calculations [27]. In fact, we can reproduce Λ-binding energies of ${}^3_\Lambda$H, ${}^4_\Lambda$He, ${}^4_\Lambda$He*, and ${}^5_\Lambda$He using the folding-model potentials with $D2'$, as shown in Appendix A. This fact realizes us the concept of the coherent $\Lambda N - \Sigma N$ coupling in s-shell hypernuclei [2].

Moreover, it should be noticed that the imaginary part of $U_{\alpha\alpha'}$ for the $\alpha\alpha'$ channel is regarded as a *spreading* potential $W_{\alpha\alpha'}$. This is significant to describe the complicated surrounding Λ excited states with all the $2N$ breakup processes, because Σ hypernuclear states can be connected with highly Λ excited states via the strong $\Lambda N - \Sigma N$ coupling. In the folding model with $D2'$, we can also reproduce the binding energy and width of ${}^4_\Sigma$He, in a comparison with the data, as shown in Appendix A.

Figure 6 displays the real and imaginary parts of the effective $2N - Y$ potential $\hat{U}_{\alpha\alpha'}(R)$ for ${}^3_Y$He ($J^\pi = 1/2^+$) at $E_\Lambda = 70$ MeV that corresponds to the Σ threshold region, as a function of the relative distance R between $2N$ and Y. We find that the coupling potentials of $\{pn\}\Sigma^+ - \{pp\}\Sigma^0$, $[pn]\Sigma^+ - \{pn\}\Sigma^+$, and $[pn]\Sigma^+ - \{pp\}\Sigma^0$ are quite strong. This nature originates from the fact that the ΣN potential has a strong isospin-spin dependence, as pointed out by Dover and Gal [40] and suggested by recent YN potential models [53]. For the imaginary parts ($W_{\alpha\alpha'}$), we also recognize that there is the spin-isospin selectivity [40] for $\Sigma N \to \Lambda N$ conversion decays. It is very important to realize whether or not the quasibound state has a narrow width in ΣNN systems. Strengths of $W_{\alpha\alpha}$ for diagonal $[pn]\Sigma^+$ and $\{pp\}\Sigma^0$ channels are -5.0 MeV and -13.2 MeV at the nuclear center, which are consistent with quenching factors $Q = 1/3$ and 1, respectively, as given in Table II of Ref. [40].

IV. RESULTS

A. ΣNN quasibound states

In order to obtain eigenvalues for bound and resonance states simultaneously, we solve the multichannel equation for the $2N - Y$ systems by the complex scaling method [54,55]. Here we use the $2N - Y$ potential given in Fig. 6 and the Coulomb force. We find that a pole position for ${}^3_\Sigma$He ($J^\pi = 1/2^+, L = 0, S = 1/2$) as a complex eigenvalue of the $2N - Y$ system, $\mathcal{E}^{(\rm pole)}_{\Sigma^+} = E_{\Sigma^+} - i\frac{1}{2}\Gamma_\Sigma$ on the second Riemann sheet $[-+++]$ that is identified by a set of four signs of [Im$k_{\{pp\}\Lambda}$, Im$k_{[pn]\Sigma^+}$, Im$k_{\{pn\}\Sigma^+}$, Im$k_{\{nn\}\Sigma^0}$] on the complex E plane. The

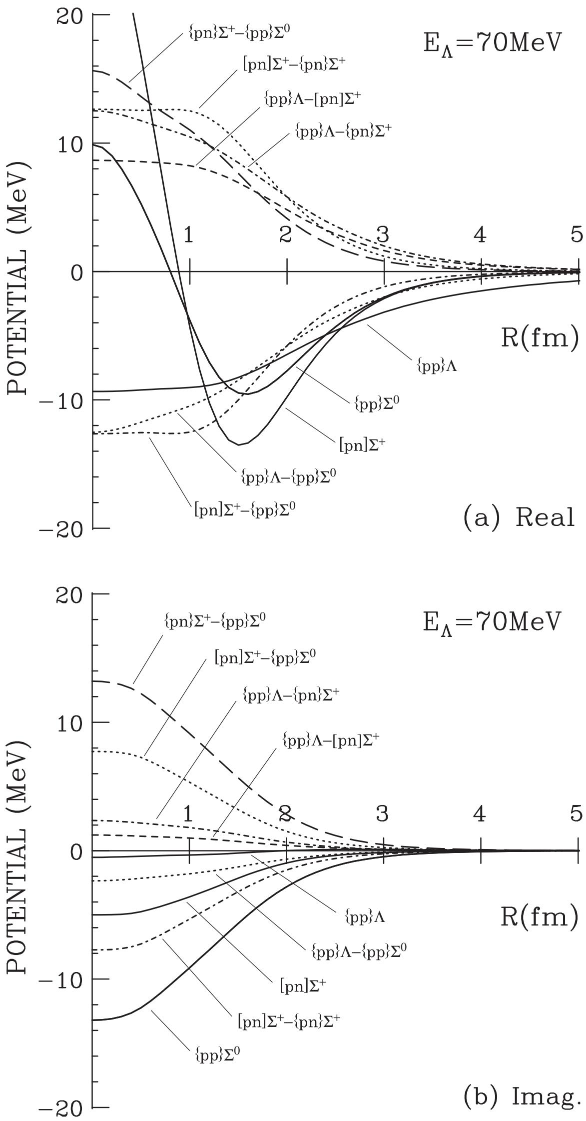

FIG. 6. (a) Real and (b) imaginary parts of the calculated effective $2N-Y$ potential $\hat{U}_{\alpha\alpha'}(R)$ for ${}^3_Y$He ($J^\pi = 1/2^+$) at $E_\Lambda = 70$ MeV in the folding-model potential, as a function of a relative distance R between $2N$ and Y.

pole is located as

$$\mathcal{E}^{(\mathrm{pole})}_{\Sigma^+}\big({}^3_\Sigma\mathrm{He}\big) = +0.96 - i\,4.5 \text{ MeV}, \tag{34}$$

where E_{Σ^+} is measured from the $d+\Sigma^+$ threshold, as shown in Table IV. Its width becomes $\Gamma_\Sigma = 9.0$ MeV. Since the pole lies in the second quadrant (Re$k_{\Sigma^+} < 0$, Im$k_{\Sigma^+} > 0$) on the complex k_{Σ^+} plane, the wave function behaves as

$$\exp(ik_{\Sigma^+}R) = \exp(i\mathrm{Re}k_{\Sigma^+}R)\exp(-\mathrm{Im}k_{\Sigma^+}R) \to 0 \tag{35}$$

in the asymptotic region ($R \to \infty$). Hence this state is identified to be a quasibound (an unstable bound) state. In the Λ region, we also confirm that there is no pole of a ${}^3_\Lambda$He bound state below the $p+p+\Lambda$ threshold.

For ${}^3_\Sigma n$ ($J^\pi = 1/2^+$, $L=0$, $S=1/2$), we find

$$\mathcal{E}^{(\mathrm{pole})}_{\Sigma^0}\big({}^3_\Sigma n\big) = -0.58 - i\,5.3 \text{ MeV}, \tag{36}$$

TABLE IV. Energies and widths of $2N-Y$ systems on complex E plane.

	(J^π, T)	E_Λ (MeV)	$E_{\Sigma^\pm}$ (MeV)	E_{Σ^0} (MeV)	Γ_Σ (MeV)	$k_{\Sigma^\pm}$ (fm^{-1})
${}^3_\Sigma$He	$(\frac{1}{2}^+, 1)$	+73.7	+0.96[a]	−3.24	9.0	$-0.322 + i0.260$
${}^3_\Sigma n$	$(\frac{1}{2}^+, 1)$	+76.4	−1.87[b]	−0.58	10.5	$-0.263 + i0.374$

[a] $E_{\Sigma^+} = E_\Lambda - 72.8$ MeV $= E_{\Sigma^0} - 4.2$ MeV, where E_{Σ^+} is measured from the ^{2}H + Σ^+ threshold.
[b] $E_{\Sigma^-} = E_\Lambda - 78.3$ MeV $= E_{\Sigma^0} + 1.3$ MeV, where E_{Σ^-} is measured from the ^{2}H + Σ^- threshold.

where E_{Σ^0} is measured from the $n+n+\Sigma^0$ threshold, and $\Gamma_\Sigma = 10.5$ MeV, as shown in Table IV.

In order to see the contributions of the $2N-Y$ components in these pole states, we calculate probabilities of isospin $T(I_2S_2)$ states for ${}^3_\Sigma$He ($T_z = +1$) and ${}^3_\Sigma n$ ($T_z = -1$):

$$P_{T(I_2S_2)} = \left|\left\langle \Psi^{T,T_z}_{(I_2S_2)} \middle| \Psi^{(\mathrm{pole})}_B \right\rangle\right|^2, \tag{37}$$

where $\Psi^{T,T_z}_{(I_2S_2)}$ is the isospin state defined in Eqs. (B1) and (B4). In Table V, we show values of $P_{T(I_2S_2)}$, together with values of probabilities on the Σ charge bases. We find that values of a sum of $P_{T=1}$ account for 99.6% and 97.9% in the ${}^3_\Sigma$He and ${}^3_\Sigma n$ states, respectively, including $\{pp\}\Lambda$ states. Hence the total isospin $T=1$ becomes an almost good quantum number.

B. π^- spectrum

Figure 7 shows the calculated inclusive spectrum of the ^{3}He(K^-, π^-) reaction at 600 MeV/c (4°) from Λ to Σ regions, together with the $J^\pi = 1/2^+$ ($L=0$, $S=1/2$) component, which is predominantly connected with $\Sigma N \to \Lambda N$ conversion processes of $[{}^3_\Sigma\mathrm{He}] \to p+p+\Lambda$ decays. The Σ hyperon produced in the real or virtual ${}^3_\Sigma$He state subsequently interacts with a second nucleon, and it is converted to a Λ via $\Sigma N \to$

TABLE V. Probabilities of channel components of the pole states of ${}^3_\Sigma$He and ${}^3_\Sigma$n with $J^\pi = 1/2^+$ on complex E plane. Calculated values are obtained by the complex scaling method.

States	Components	Probabilities (%)
${}^3_\Sigma$He	$\{pp\}\Lambda$	2.07
	$[pn]\Sigma^+$	54.9
	$\{pn\}\Sigma^+$	24.7
	$\{pp\}\Sigma^0$	18.3
	$T=1\,(I_2=0, S_2=1)$	54.9
	$T=1\,(I_2=1, S_2=0)$	42.5
	$T=2$	0.45
${}^3_\Sigma n$	$\{nn\}\Lambda$	2.42
	$[pn]\Sigma^-$	39.5
	$\{pn\}\Sigma^-$	20.9
	$\{nn\}\Sigma^0$	37.2
	$T=1\,(I_2=0, S_2=1)$	39.5
	$T=1\,(I_2=1, S_2=0)$	56.0
	$T=2$	2.10

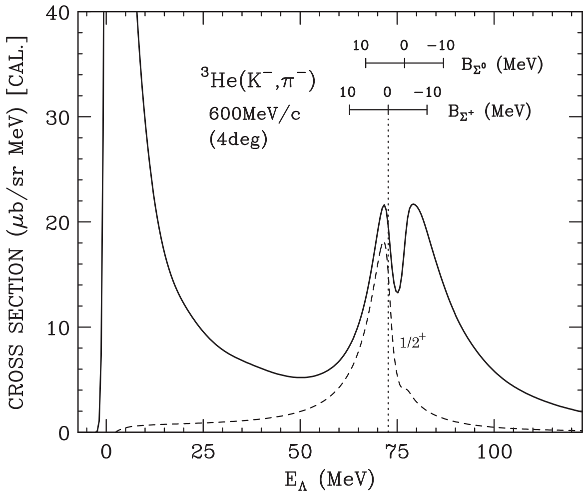

FIG. 7. Calculated inclusive π^- spectrum of the ^{3}He(K^-, π^-) reaction at 600 MeV/c (4°). The solid curve denotes the total spectrum, and the dashed curve denotes the $J^\pi = 1/2^+$ ($L = 0$, S =1/2) component caused by conversion decay processes as $[^3_\Sigma\text{He}] \to p + p + \Lambda$, with a detector resolution of 2 MeV FWHM.

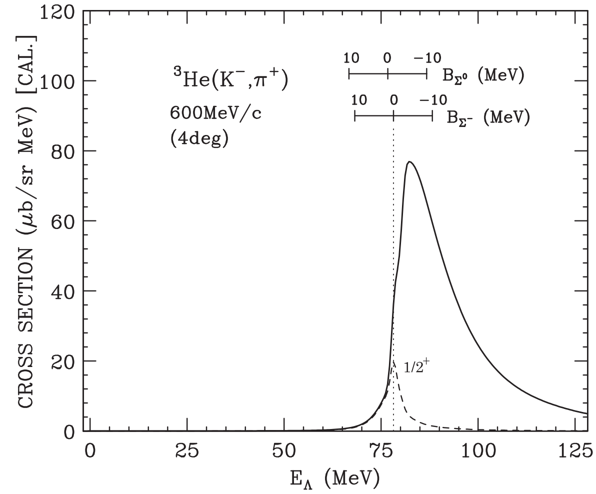

FIG. 9. Calculated inclusive π^+ spectrum of the ^{3}He(K^-, π^+) reaction at 600 MeV/c (4°). The solid curve denotes the total spectrum, and the dashed curve denotes the $J^\pi = 1/2^+$ ($L = 0$, $S = 1/2$) component caused by conversion decay processes as $[^3_\Sigma n] \to n + n + \Lambda$, with a detector resolution of 2 MeV FWHM.

ΛN conversion processes inducing $2N$-nuclear breakup due to the mass difference $m_\Sigma - m_\Lambda \simeq 77$ MeV. It is recognized that a clear peak just below the $d + \Sigma^+$ threshold in the π^- spectrum, which corresponds to the $^3_\Sigma$He quasibound state with $J^\pi = 1/2^+$, $T \simeq 1$ on the Riemann sheet [−+++] near the Σ threshold. Such a $\Sigma N \to \Lambda N$ conversion spectrum with $p + p + \Lambda$ may give evidence of the existence of the $^3_\Sigma$He quasibound state.

In the π^- spectrum we obtain the decomposition of the inclusive spectrum into partial spectra of the $\{pp\}\Lambda$, $[pn]\Sigma^+$, $\{pn\}\Sigma^+$ and $\{pp\}\Sigma^0$ components, as given in Eq. (25). Figure 8 illustrates the contributions of the Λ-emitted processes of $\{pp\}\Lambda$ and $[^3_\Sigma\text{He}] \to p + p + \Lambda$ conversion near the Σ threshold, together with those of the Σ-emitted processes of $[pn]\Sigma^+$, $\{pn\}\Sigma^+$, and $\{pp\}\Sigma^0$. For the Σ continuum region, we find that the contribution of the $\{pp\}\Sigma^0$ component is larger than that of the $[pn]\Sigma^+$ component because the production amplitudes have $|\overline{f}_{(\Sigma^0\pi^-)}| \gg |\overline{f}_{(\Sigma^+\pi^-)}|$ near $p_{K^-} = 600$ MeV/c [5]. Below the $d + \Sigma^+$ threshold, the $^3_\Sigma$He quasibound state is predominantly populated via the Σ^0 components by $\overline{f}_{(\Sigma^0\pi^-)}$.

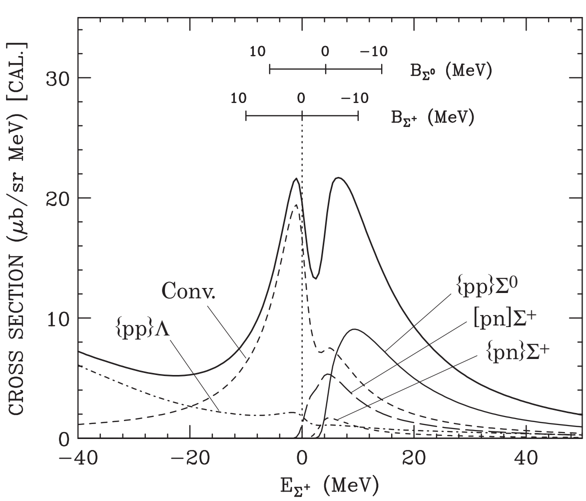

FIG. 8. The decomposition of the calculated inclusive π^- spectrum of the ^{3}He(K^-, π^-) reaction at 600 MeV/c (4°) near the Σ threshold, together with the components of $\{pp\}\Lambda$, $[pn]\Sigma^+$, $\{pn\}\Sigma^+$, $\{pp\}\Sigma^0$, and $[^3_\Sigma\text{He}] \to p + p + \Lambda$ conversion processes, obtained by folding with a detector resolution of 2 MeV FWHM.

C. π^+ spectrum

The nuclear (K^-, π^+) reaction at forward direction of $p_{K^-} = 600$ MeV/c seems to be appropriate to search a bound state in the Σ bound region. The reasons were because (i) this reaction can populate only the Σ^- components in the final states by its double-charge exchange reaction, so that the contribution of a Λ hyperon is removed out from the π^+ spectrum, and (ii) it has a substitutional mechanism under the near-recoilless condition so as to produce the $^3_\Sigma n$ quasibound state from ^{3}He, as well as the $^3_\Sigma$He quasibound state in the (K^-, π^-) reaction. Therefore, we have naively expected that a signal of the corresponding peak can be clearly observed in the π^+ spectrum, rather than the π^- one.

Figure 9 shows the calculated inclusive spectrum of the ^{3}He(K^-, π^+) reaction at 600 MeV/c (4°) from Λ to Σ regions, together with the $J^\pi = 1/2^+$ ($L = 0$, $S = 1/2$) component in $[^3_\Sigma n] \to n + n + \Lambda$ conversion processes, obtained by folding with a detector resolution of 2 MeV FWHM. Surprisingly, we find that although the $^3_\Sigma n$ quasibound state exists, the corresponding peak disappears in the inclusive π^+ spectrum, where the component of the Σ quasibound state is quite reduced rather than that of Σ continuum states.

Figure 10 illustrates the contributions of the $[^3_\Sigma n] \to n + n + \Lambda$ conversion, $\{nn\}\Sigma^0$, $[pn]\Sigma^-$, and $\{pn\}\Sigma^-$ processes near the Σ threshold. Because these states can be populated via

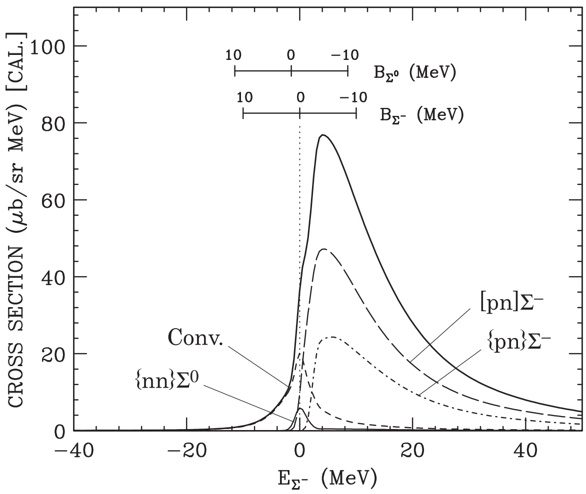

FIG. 10. The decomposition of the calculated inclusive π^+ spectrum of the ^{3}He(K^-,π^+) reaction at 600 MeV/c (4°) near the Σ threshold, together with the components of $[pn]\Sigma^-$, $\{pn\}\Sigma^-$, $\{nn\}\Sigma^0$, and $[^3_\Sigma n] \to n + n + \Lambda$ conversion processes, obtained by folding with a detector resolution of 2 MeV FWHM.

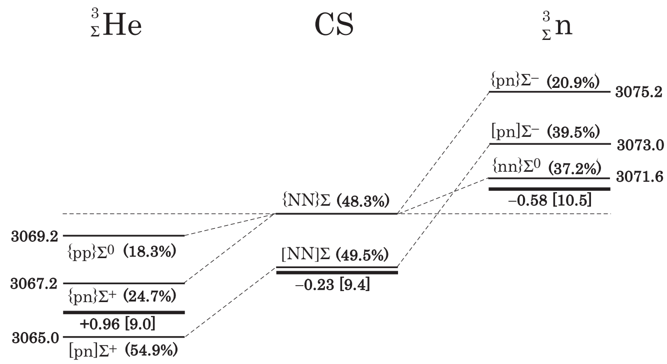

FIG. 11. Energies and widths of the ΣNN quasibound states (thick line) near the Σ threshold. The square brackets denote the widths of the quasibound states, and the round brackets denote probabilities of each channel component. See also Tables IV and V.

only Σ^- productions by $\overline{f}_{(\Sigma^-\pi^+)}$ in the (K^-,π^+) reaction. We find that the $[pn]\Sigma^-$ and $\{pn\}\Sigma^-$ components predominantly occur in Σ continuum regions, and that a small $\{nn\}\Sigma^0$ component can be populated via the quasibound state near the $n+n+\Sigma^0$ threshold, followed by $[^3_\Sigma n] \to n+n+\Sigma^0$.

V. DISCUSSION

A. Charge symmetry breaking

It is noticed that the $^3_\Sigma$He and $^3_\Sigma n$ quasibound states belong to $J^\pi = 1/2^+$ isotriplet states in ΣNN systems, whereas a value of $\mathcal{E}^{(\rm pole)}_{\Sigma^+}$ for $^3_\Sigma$He slightly differs from that of $\mathcal{E}^{(\rm pole)}_{\Sigma^-}$ for $^3_\Sigma n$, as seen in Table IV. This discrepancy comes from the Σ threshold energy difference and the Coulomb force, leading to the charge symmetry breaking (CSB) in the ΣNN systems. We study a dependence of these pole positions and configurations of the $2N - Y$ quasibound states on CSB effects

To see the CSB effects, we obtain a charge symmetric (CS) state, neglecting the Coulomb force and replacing masses of $m_{\Sigma^{\pm,0}}$ and $m_{p,n}$ by averaged masses of $\overline{m}_\Sigma = 1193.2$ MeV and $\overline{m}_N = 938.9$ MeV, respectively. We find

$$\mathcal{E}^{(\rm pole)}_{\Sigma}({\rm CS}) = -0.23 - i\,4.7\ {\rm MeV}, \tag{38}$$

and probabilities of the $[NN]\Sigma$, $\{NN\}\Sigma$, and $\{NN\}\Lambda$ components that account for 49.5%, 48.25%, and 2.3%, respectively. Although the threshold energy difference between $pn\Sigma^+$ and $pp\Sigma^0$ ($nn\Sigma^-$ and $pn\Sigma^0$) amounts to 2.0 (−3.6) MeV, we find that the energy levels for $^3_\Sigma$He ($^3_\Sigma n$) is +0.96 (−0.58) MeV, which is slightly different from −0.23 MeV obtained for CS. This confirms the fact that the ΣNN quasibound states have a $T \simeq 1$ good isospin (97%–99%). We obtain that the width for $^3_\Sigma$He amounts to 9.0 MeV, which is slightly smaller than 9.4 MeV for CS because the $pp\Sigma^0$ threshold is located above the $d + \Sigma^+$ one. Contrary to $^3_\Sigma$He, the width of $^3_\Sigma n$ becomes broader up to 10.5 MeV because the $nn\Sigma^0$ threshold is located below the $d + \Sigma^-$ threshold. Figure 11 illustrates energy levels and widths of the ΣNN quasibound states for $^3_\Sigma$He and $^3_\Sigma n$ near the Σ threshold, together with the probabilities of the $2N - Y$ components in the ΣNN systems. We also confirmed that the CSB effects rarely have an influence on the shape and magnitude of the $\pi^\mp$ spectra.

B. Interference effects between production amplitudes

It should be noticed that a production cross section near the Σ threshold is very sensitive not only to the pole position but also to the configuration of the wave function of the quasibound state. We consider difference of the Σ production mechanism between the π^- and π^+ spectra in terms of interference among Σ production amplitudes. In order to understand the behavior of the $\pi^\mp$ spectra, we evaluate interference effects among configurations of the NN core states in Σ production amplitude, because the $2N - Y$ potential should admix $^3S_1$ and $^1S_0$ states in the NN pair [18], depending on the nature of the ΣN potential.

In the π^- spectrum, production amplitude for $^3_\Sigma$He near the Σ threshold is approximately written as

$$\begin{aligned}
&\langle ^3_\Sigma{\rm He}\,\pi^-|T|^3{\rm He}K^-\rangle \\
&\quad\simeq \frac{1}{\sqrt{2}}\left\{\frac{1}{\sqrt{2}}\overline{f}_{(\Sigma^+\pi^-)} - \overline{f}_{(\Sigma^0\pi^-)}\right\}\left\langle\Psi^{2,1}_{(s)}\middle|\Psi(^3{\rm He})\right\rangle \\
&\qquad+\left\{\frac{\sqrt{3}+1}{2}\overline{f}_{(\Sigma^+\pi^-)} + \frac{1}{2}\overline{f}_{(\Sigma^0\pi^-)}\right\}\langle\Psi^{1,1}_{(-)}|\Psi(^3{\rm He})\rangle \\
&\qquad+\left\{\frac{\sqrt{3}-1}{2}\overline{f}_{(\Sigma^+\pi^-)} - \frac{1}{2}\overline{f}_{(\Sigma^0\pi^-)}\right\}\langle\Psi^{1,1}_{(+)}|\Psi(^3{\rm He})\rangle
\end{aligned} \tag{39}$$

on isospin bases, where $\Psi^{T,T_z}_{(I_2S_2)}$ is the isospin state defined in Eq. (B1). The wave function of $\Psi^{1,1}_{(-)}$ is regarded as that of a $^3_\Sigma$He ground state with $J^\pi = 1/2^+$, $T = 1$, and $\Psi^{1,1}_{(+)}$ as a $^3_\Sigma$He* excited state. The relative phase between $\overline{f}_{(\Sigma^+\pi^-)}$ and $\overline{f}_{(\Sigma^0\pi^-)}$ is $\varphi(\Sigma^+/\Sigma^0) = +4.8°$ at $p_{K^-} = 600$ MeV/c, so the component of $\Psi^{1,1}_{(-)}$ is relatively enhanced in the π^- spectrum. We recognize that the interference effects between $\overline{f}_{(\Sigma^+\pi^-)}$ and

$\overline{f}_{(\Sigma^0\pi^-)}$ play an important role in populating the component of $\Psi^{1,1}_{(-)}$.

In the π^+ spectrum, on the other hand, production amplitude for ${}^3_\Sigma n$ near the Σ threshold is approximately written as

$$\begin{aligned}\langle {}^3_\Sigma n\,\pi^+ | T | {}^3\mathrm{He}K^-\rangle \\ \simeq \overline{f}_{(\Sigma^-\pi^+)}\bigg\{ \frac{1}{2}\langle \Psi^{2,-1}_{(s)} | \Psi({}^3\mathrm{He})\rangle + \frac{2\sqrt{3}-\sqrt{2}}{4}\langle \Psi^{1,-1}_{(-)}|\Psi({}^3\mathrm{He})\rangle \\ + \frac{2\sqrt{3}+\sqrt{2}}{4}\langle \Psi^{1,-1}_{(+)}|\Psi({}^3\mathrm{He})\rangle \bigg\} \end{aligned} \tag{40}$$

on isospin bases. We find that a cross section for $\Psi^{1,-1}_{(-)}$ as the ${}^3_\Sigma n$ ground state is relatively reduced by a factor $[(2\sqrt{3}-\sqrt{2})/4]^2 = 0.51^2 \simeq 0.26$, whereas that for $\Psi^{1,-1}_{(+)}$ as a ${}^3_\Sigma n^*$ excited state is enhanced by a factor $[(2\sqrt{3}+\sqrt{2})/4]^2 = 1.22^2 \simeq 1.49$. The interference effects are considered as *dynamical* ones caused by ${}^3S_1 - {}^1S_0$ admixture in the NN pair for the ΣNN systems. This mechanism originates from properties of the ΣN interaction, and it is inevitable whenever we consider the ^{3}He(K^-,π^+) reaction. In Appendix B, we discuss in detail the interference effects.

C. Dependence of the $\pi^\mp$ spectra on Σ widths

Several three-body YNN calculations suggested that there is a quasibound state in ΣNN systems. However, the Σ width is unsettled because the ΣN potential still remains quantitative ambiguities. It seems that the shape and magnitude of the peak for the ΣNN quasibound state is very sensitive to a value of its width. We demonstrate behavior of the $\pi^\mp$ spectrum near the Σ threshold in order to compare it with experimental observations. We introduce an artificial factor of f_W changing the strength of the spreading potential:

$$W_{\alpha\alpha'} \to f_W \times W_{\alpha\alpha'}. \tag{41}$$

Here let us consider several cases of various widths in the $\pi^\mp$ spectrum as follows:

(i) Case A was obtained by $f_W = 1.00$, leading to a broad width of $\Gamma_\Sigma \simeq 9$ MeV. This width was suggested by a Faddeev calculation for the $\Lambda + d \to \Sigma + N + N$ scattering near the Σ threshold by Afnan and Gibson [16].

TABLE VI. Energies and widths of the ${}^3_\Sigma$He quasibound state with $J^\pi = 1/2^+, T \simeq 1$ on complex energy plane when the spreading potential $W_{\alpha\alpha'}$ is artificially changed.

Case	f_W	E_{Σ^+} (MeV)	E_{Σ^0} (MeV)	Γ_Σ (MeV)	k_{Σ^+} (fm^{-1})
A	1.00	+0.96	−3.24	9.0	$-0.322 + i0.260$
B	0.75	−0.10	−4.30	6.9	$-0.249 + i0.257$
C	0.50	−0.94	−5.14	4.8	$-0.176 + i0.257$
D	0.25	−1.53	−5.73	2.8	$-0.101 + i0.259$

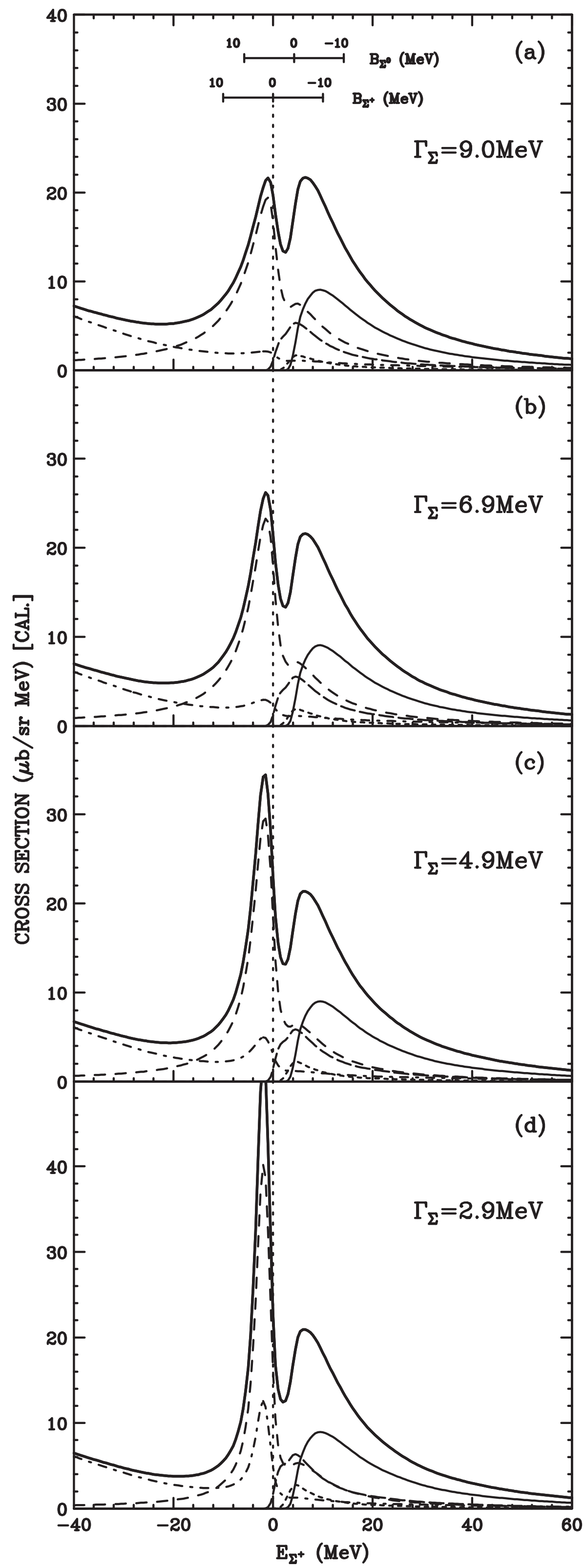

FIG. 12. Shape dependence of the calculated π^- spectrum in the ^{3}He(K^-, π^-) reaction near the Σ threshold at 600 MeV/c (4°), when changing the spreading potential $W_{\alpha\alpha'}$ artificially by f_W = (a) 1.00, (b) 0.75, (c) 0.50, and (d) 0.25, which correspond to widths of Γ_Σ = 9.0, 6.9, 4.9, and 2.9 MeV, respectively. These spectra are obtained by folding with a detector resolution of 2 MeV FWHM.

TABLE VII. Energies and widths of the ${}^{3}_{\Sigma}n$ quasibound state with $J^{\pi} = 1/2^{+}$, $T \simeq 1$ on complex energy plane when the spreading potential $W_{\alpha\alpha'}$ is artificially changed.

Case	f_W	E_{Σ^-} (MeV)	E_{Σ^0} (MeV)	Γ_Σ (MeV)	k_{Σ^-} (fm^{-1})
A	1.00	−1.87	−0.58	10.5	$-0.263 + i0.374$
B	0.75	−2.79	−1.50	8.1	$-0.200 + i0.380$
C	0.50	−3.51	−2.22	5.7	$-0.138 + i0.388$
D	0.25	−4.02	−2.73	3.2	$-0.077 + i0.396$

(ii) Case B was obtained by $f_W = 0.75$, leading to $\Gamma_\Sigma \simeq$ 7 MeV, of which width was predicted in three-body calculations within a SAP approximation by Koike and Harada [18].

(iii) Case C was obtained by $f_W = 0.50$, leading to $\Gamma_\Sigma \simeq$ 5 MeV, which is equivalent to a half of the width of Case A.

(iv) Case D was obtained by $f_W = 0.25$, leading to a narrow Σ width of $\Gamma_\Sigma \simeq$ 2–3 MeV in recent Faddeev $\Lambda NN - \Sigma NN$ calculations using NN and YN potentials derived from a chiral constituent quark models by Garcilazo *et al.* [19].

In Table VI, we obtain the calculated values of energies and widths of the ${}^{3}_{\Sigma}$He quasibound state on the complex E plane. Figure 12 shows dependence of the shape and magnitude of the π^- spectrum on the width. In Case A, we confirm that a peak of the π^- spectrum is enhanced just below the $d + \Sigma^+$ threshold, as already seen in Fig. 8. In Case B, we also recognize that the peak can be observed as a candidate of the Σ hypernuclear bound state, having a narrow width of $\Gamma_\Sigma \simeq$ 7 MeV. This is equivalent to the value of $\langle v\sigma_{\Sigma^- p\to\Lambda n}\rangle_{\rm av}$, where v and $\sigma_{\Sigma^- p\to\Lambda n}$ are the velocity and total cross section data of $\Sigma^- p \to \Lambda n$ at low energies, respectively. In Cases C and D, we find that a peak of the quasibound state is more clearly observed below the Σ threshold, so that it might be a very good candidate if the ΣNN quasibound state has such a narrow width. Consequently, the π^- spectrum near the Σ threshold provides valuable information to understand the nature of ΣN potentials and the structure of the ΣNN quasibound state.

In Table VII, we obtain the calculated values of energies and widths of the ${}^{3}_{\Sigma}n$ quasibound state on the complex E plane. Figure 13 shows the shape and magnitude of the π^+ spectrum on the corresponding widths. In Cases A and B, we find that the shape of the spectrum is scarcely changed by a value of f_W. This originates from the fact that the contributions of the $[pn]\Sigma^-$ and $\{pn\}\Sigma^-$ components predominantly occur in continuum states, and the shape of continuum spectrum is insensibly influenced by the spreading potential $W_{\alpha\alpha'}$. For Case D, the quasibound state has a very narrow width of $\Gamma_\Sigma \simeq$ 3 MeV, observed below the $n + n + \Sigma^0$ threshold. However, the cross section of the quasibound state is rather small, compared with the continuum one, because of a reduction mechanism caused by the interference effects in the π^+ spectrum, as discussed in Sec. V B.

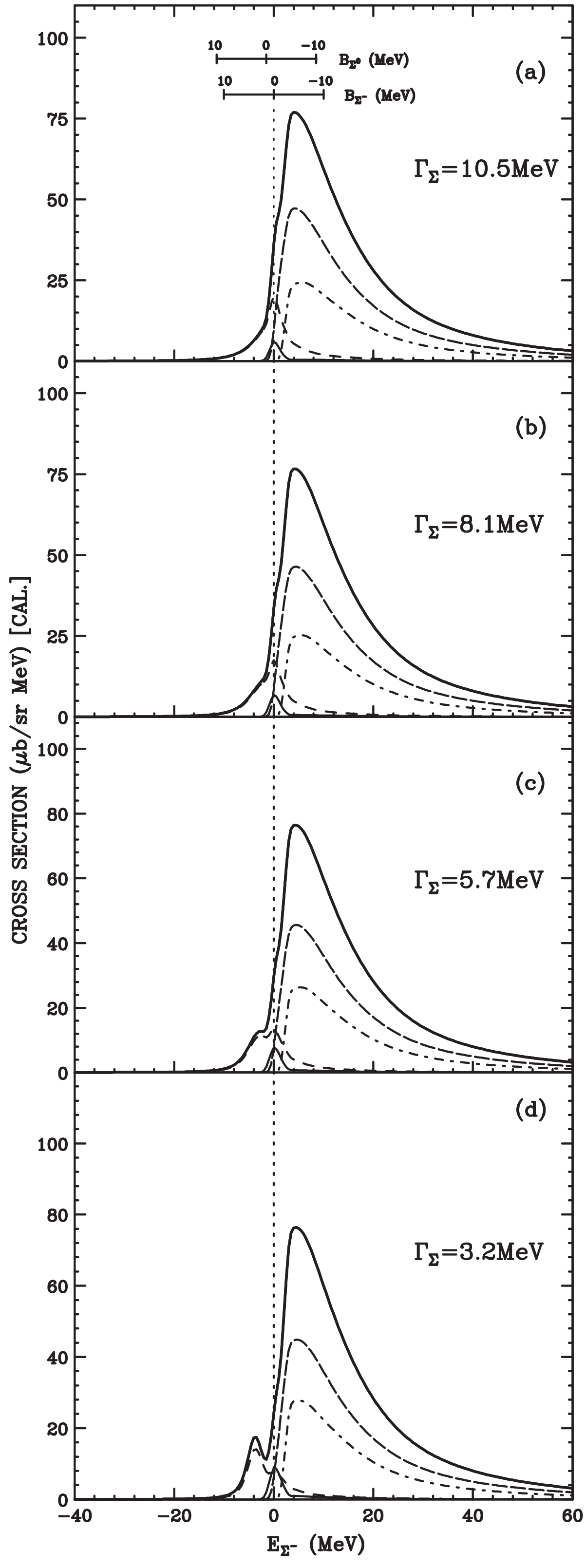

FIG. 13. Shape dependence of the calculated π^+ spectrum in the ^{3}He(K^-, π^+) reaction near the Σ threshold at 600 MeV/c (4°), when changing the spreading potential $W_{\alpha\alpha'}$ artificially by $f_W =$ (a) 1.00, (b) 0.75, (c) 0.50, and (d) 0.25, which correspond to widths of $\Gamma_\Sigma = 10.5$, 8.1, 5.7, and 3.2 MeV, respectively. These spectra are obtained by folding with a detector resolution of 2 MeV FWHM.

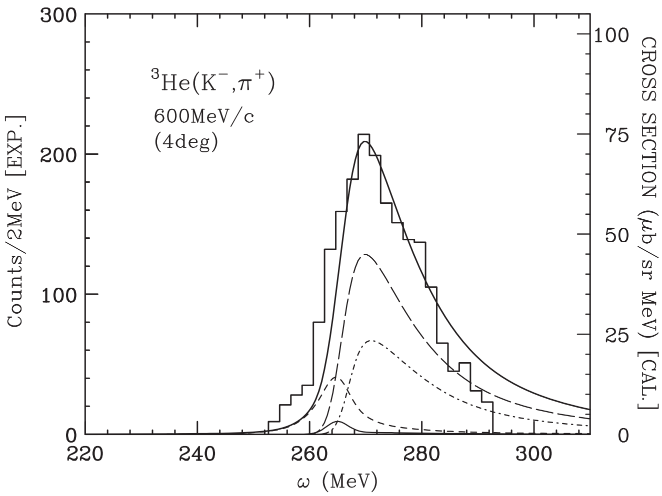

FIG. 14. Comparison of the calculated π^+ spectrum with the experimental data in the ^{3}He(K^-, π^+) reaction at 600 MeV/c (4°). The bold solid curve denotes the inclusive π^+ spectrum obtained by folding with a detector resolution of 5 MeV FWHM. The dashed, long-dashed, dot-dashed, and thin-solid curves denote the contribution of the $[^3_\Sigma n] \to n + n + \Lambda$ decay, $[pn]\Sigma^-$, $\{pn\}\Sigma^-$, and $\{nn\}\Sigma^0$ components, respectively. Data are taken from BNL-E774 [20].

D. Comparison with experimental data

It has been recognized that there is no evidence of a narrow structure for the ΣNN quasibound state ($^3_\Sigma n$) below the Σ threshold in the ^{3}He(K^-, π^+) reaction from E774 experiments at BNL [20]. Figure 14 shows the calculated inclusive π^+ spectrum at $p_{K^-} = 600$ MeV/c (4°), in order to be compared with the BNL-E774 data [20]. Here the spectrum was obtained by folding with a detector resolution of 5 MeV FWHM. We find that the calculated π^+ spectrum is in good agreement with the data. Because the shape of the spectrum is not so sensitive to its width, it seems that it is difficult to extract information on the width of the quasibound state from the data in the π^+ spectrum. Consequently, contradictory arguments against the existence of a ΣNN bound state may be settled in our calculations.

VI. SUMMARY AND CONCLUSIONS

We have theoretically demonstrated the inclusive and semiexclusive spectra in the ^{3}He(K^-, $\pi^\mp$) reactions at 600 MeV/c (4°) within the DWIA, using the coupled $(2N - \Lambda) + (2N - \Sigma)$ model with the spreading potential. The effective $2N - Y$ potential derived from YN g-matrices has strong isospin-spin dependence, and provides quasibound states ($^3_\Sigma$He, $^3_\Sigma$H, $^3_\Sigma n$) with $J^\pi = 1/2^+$ ($L = 0$, $S = 1/2$), $T \simeq 1$ near the Σ threshold. The results are summarized as follows:

(i) The coupled-channel framework is essential for calculating the inclusive π^- and π^+ spectra of the ^{3}He(K^-, $\pi^\mp$) reactions, in order to consider significant effects of interference between $K^- + N \to \pi + Y$ amplitudes and the threshold energy differences.

(ii) The effective $2N - Y$ potential is constructed by a folding-model potential with YN g-matrices derived from the central $D2'$ potential, which is simulated to the Nijmegen model D. Such folding potentials can overcome serious overbinding problems in s-shell Λ hypernuclei.

(iii) The calculated inclusive spectrum of the ^{3}He(K^-, π^-) reaction shows a signal of the $^3_\Sigma$He quasibound state with $J^\pi = 1/2^+$, $T = 1$ near the Σ threshold, and its width has $\Gamma_\Sigma \simeq 9$ MeV.

(iv) The calculated inclusive spectrum of the ^{3}He(K^-, π^+) reaction shows no peak of the $^3_\Sigma n$ quasibound state that is located near the Σ threshold with $\Gamma_\Sigma = 10.5$ MeV, by interference effects caused by $^3S_1 - {}^1S_0$ admixture in the NN pair for $^3_\Sigma n$ and the CSB effects. This spectrum is consistent with the BNL-E774 data.

In conclusion, we show that a signal of the $^3_\Sigma$He quasibound state is clearly confirmed near the Σ threshold in the π^- spectrum, whereas the peak of the $^3_\Sigma n$ quasibound state is relatively reduced in the π^+ spectrum. We believe that the π^- and π^+ spectra on ^{3}He targets provide valuable information on properties of ΣNN quasibound states so as to study the ΣN interaction.

ACKNOWLEDGMENTS

The authors would like to thank Professor T. Fukuda, Professor Y. Akaishi, Professor H. Tamura, and Dr. T. Koike for many valuable discussions. This work was supported by JSPS KAKENHI Grant Nos. 24105008 and 25400278.

APPENDIX A: BINDING ENERGIES OF s-SHELL Λ HYPERNUCLEI IN FOLDING-MODEL CALCULATIONS

Let us consider Λ binding energies of $^3_\Lambda$H, $^4_\Lambda$He, $^4_\Lambda$He*, and $^5_\Lambda$He in folding models. We obtain YN g-matrices in Eq. (32), solving the coupled Bethe-Goldstone equation

$$\begin{bmatrix}\Psi_\Lambda \\ \Psi_\Sigma\end{bmatrix} = \begin{bmatrix}\Phi_\Lambda \\ 0\end{bmatrix} + \frac{Q}{e} v \begin{bmatrix}\Psi_\Lambda \\ \Psi_\Sigma\end{bmatrix}, \tag{A1}$$

where e and Q are the energy denominator and Pauli exclusion operator, respectively [50,51]. v is a YN potential including the $\Lambda N - \Sigma N$ coupling. The $D2$ potential [2] is a central YN potential that simulates the Nijmegen model D [23]. The $D2'$ potential we used in this paper is a modified version to reproduce the experimental value of $B_\Lambda(^5_\Lambda\text{He})$, multiplying the strength of the long-range part in the ΣN $^3S_1$ by a factor (0.954) [27]. In Table VIII, we show the calculated results of Λ binding energies of s-shell Λ hypernuclei in the folding models. We obtain $B_\Lambda = 0.13$, 2.4, 1.1, and 3.1 MeV for $^3_\Lambda$H, $^4_\Lambda$He, $^4_\Lambda$He*, and $^5_\Lambda$He, respectively. Here parameters of starting energies and Fermi momentum were taken to be (E_s, $k_{\rm F}$) = (−2.2 MeV, 1.05 fm^{-1}), (−8 MeV, 1.05 fm^{-1}), (−8 MeV, 1.05 fm^{-1}), and (−28 MeV, 1.30 fm^{-1}) for $^3_\Lambda$H, $^4_\Lambda$He, $^4_\Lambda$He*, and $^5_\Lambda$He, respectively. In order to compare them with the experimental data [56], we need to include rearrangement energies by $-\kappa_N U_{\alpha\alpha'}$ [57,58] where we choose $\kappa_N = 0.06$, 0.08, 0.08, and 0.115 for $^3_\Lambda$H, $^4_\Lambda$He, $^4_\Lambda$He*, and $^5_\Lambda$He, respectively. We confirm that the calculated values of B_Λ can reasonably

TABLE VIII. Binding energies and Σ-mixing probabilities of s-shell Λ hypernuclei in the folding-model potential calculations for g-matrices with the *YN* $D2'$ potential, together with those obtained in Brueckner-Hartree-Fock [2] and SVM calculations [25,27]. Data are taken from Ref. [56].

	${}^{3}_{\Lambda}$H $(1/2^+)$		${}^{4}_{\Lambda}$He (0^+)		${}^{4}_{\Lambda}$He* (1^+)		${}^{5}_{\Lambda}$He $(1/2^+)$	
	B_Λ (MeV)	P_Σ (%)	B_Λ (MeV)	P_Σ (%)	B_Λ (MeV)	P_Σ (%)	B_Λ (MeV)	P_Σ (%)
This work[a]								
with $-\kappa_N U$[b]	0.13	0.07	2.4	2.0	1.1	0.02	3.1	–
w/o $-\kappa_N U$	0.26	0.10	3.0	2.1	1.5	0.03	4.4	–
BHF [2]			2.4	1.9	1.1	0.01	3.1	–
SVM [25,27]	0.056	0.14	2.23	1.85	0.91	0.42	3.18	0.61
Expt. [56]	0.13 ± 0.05		2.39 ± 0.03		1.24 ± 0.04		3.12 ± 0.02	

[a]Starting energies and Fermi momenta are used as $(E_S,\ k_{\rm F}) = (-2.2$ MeV, 1.05 fm$^{-1})$, $(-8$ MeV, 1.05 fm$^{-1})$, $(-8$ MeV, 1.05 fm$^{-1})$, and $(-28$ MeV, 1.30 fm$^{-1})$ for ${}^{3}_{\Lambda}$H, ${}^{4}_{\Lambda}$He, ${}^{4}_{\Lambda}$He*, and ${}^{5}_{\Lambda}$He, respectively.
[b]Correction of rearrangement energies is taken from $-\kappa_N U$ [57,58], where we choose $\kappa_N = 0.06$, 0.08, 0.08, and 0.115 for ${}^{3}_{\Lambda}$H, ${}^{4}_{\Lambda}$He, ${}^{4}_{\Lambda}$He*, and ${}^{5}_{\Lambda}$He, respectively.

reproduce the corresponding experimental data. This fact supports the importance of the coherent $\Lambda N - \Sigma N$ coupling in s-shell hypernuclei [2]. It should be noticed that our folding-model calculations provide to explain properties of the s-shell hypernuclei, whereas the values of P_Σ for ${}^{4}_{\Lambda}$He* and ${}^{5}_{\Lambda}$He should be in disagreement with those of SVM because no D-wave component is included in our model space.

In order to describe properties of Σ hypernuclei, we must consider the binding energy and width of a ${}^{4}_{\Sigma}$He quasibound state with $J^\pi = 0^+$, $T = 1/2$. Let us calculate a pole position of ${}^{4}_{\Sigma}$He which is located on the complex E plane by the complex scaling method [54,55], when we use $(E_S,\ k_{\rm F}) = (-8$ MeV, 1.05 fm$^{-1})$ and $\kappa_N = 0.08$ as the parameters in folding-model calculations. In Table IX, we show the calculated result of the binding energy and width, in order to be compared with those of experimental data [9,10]. We find $B_{\Sigma^+} = 0.89$ MeV and $\Gamma_\Sigma = 11.8$ MeV with *YN* g-matrices derived from the $D2'$ potential where $E_{\Sigma^+} = -B_{\Sigma^+} - i\frac{1}{2}\Gamma_\Sigma$ where B_{Σ^+} is measured from the ^{3}H $+ \Sigma^+$ threshold.

TABLE IX. Binding energy and width of the ${}^{4}_{\Sigma}$He quasibound state with $J^\pi = 0^+$, $T = 1/2$ in the folding-model potential calculations for g-matrices with the *YN* $D2'$ potential, in a comparison with analysis of theoretical calculation [31] and experimental data taken from Refs. [9,10].

	B_{Σ^+}[b] (MeV)	Γ_Σ[b] (MeV)
This work[a]	0.83	11.8
Harada [31]	1.1	12.4
Outa *et al.* [9]	2.8 ± 0.7	12.1 ± 1.2
Nagae *et al.* [10]	$4.4 \pm 0.3 \pm 1$	$7.0 \pm 0.7^{+1.2}_{-0.0}$

[a]Starting energy and Fermi momentum of $(E_S,\ k_{\rm F}) = (-8$ MeV, 1.05 fm$^{-1})$, and the rearrangement energy with $\kappa_N = 0.08$ are used.
[b]$E_{\Sigma^+} = -B_{\Sigma^+} - i\frac{1}{2}\Gamma_\Sigma$ determined on complex E plane, where B_{Σ^+} is measured from the ^{3}H $+ \Sigma^+$ threshold.

APPENDIX B: PRODUCTION AMPLITUDES FOR $(K^-, \pi^\mp)$ REACTIONS ON ISOSPIN ΣNN STATES

In order to understand behavior of the $\pi^\mp$ spectra, we consider Σ production amplitudes for isospin ΣNN states in ^{3}He$(K^-, \pi^\mp)$ reactions. In the π^- spectrum, we recognize that the ${}^{3}_{\Sigma}$He quasibound state is populated via $\overline{f}_{(\Lambda\pi^-)}$, $\overline{f}_{(\Sigma^+\pi^-)}$, and $\overline{f}_{(\Sigma^0\pi^-)}$, and this state is identified by a configuration of $\Psi^{T,T_z}_{(I_2 S_2)}$. We obtain

$$\begin{aligned}
\Psi^{2,1}_{(s)} &= \frac{1}{\sqrt{2}}|\{pp\}\Sigma^0\rangle + \frac{1}{\sqrt{2}}|\{pn\}\Sigma^+\rangle, \\
\Psi^{1,1}_{(s)} &= \frac{1}{\sqrt{2}}|\{pp\}\Sigma^0\rangle - \frac{1}{\sqrt{2}}|\{pn\}\Sigma^+\rangle, \\
\Psi^{1,1}_{(t)} &= |[pn]\Sigma^+\rangle.
\end{aligned} \tag{B1}$$

where s and t denote spin-singlet ($I_2 = 1$, $S_2 = 0$) and spin-triplet ($I_2 = 0$, $S_2 = 1$) states, respectively, for the $2N$ pair in the ΣNN systems. Therefore, we have total isospin $T = 1$ good states as

$$\Psi^{1,1}_{(\pm)} = a\Psi^{1,1}_{(s)} \pm b\Psi^{1,1}_{(t)}, \tag{B2}$$

owing to the strong admixture of $(I_2, S_2) = (0,1)$ and $(1,0)$ states in the NN pair. Because the $2N - Y$ potential should admix ${}^3S_1$ and ${}^1S_0$ states in the NN pair, depending on the nature of the ΣN potential [18], interference effects of Σ production amplitude are important to make a shape of the π^- spectrum. As seen in Sec. V A, when $a = b = 1/\sqrt{2}$ for simplicity we obtain $\Psi^{1,1}_{(-)}$ that corresponds to the ground state in ${}^{3}_{\Sigma}$He, and $\Psi^{1,1}_{(+)}$ to an excited state. If we approximately omit Λ production amplitude of $\overline{f}_{(\Lambda\pi^-)}$ in the Σ threshold region, we obtain production amplitude for the (K^-, π^-) reaction as

$$\begin{aligned}
&\langle {}^{3}_{\Sigma}\mathrm{He}\,\pi^- | T | {}^3\mathrm{He} K^- \rangle \\
&\quad \simeq \frac{1}{\sqrt{2}}\left\{\frac{1}{\sqrt{2}}\overline{f}_{(\Sigma^+\pi^-)} - \overline{f}_{(\Sigma^0\pi^-)}\right\}\langle \Psi^{2,1}_{(s)} | \Psi({}^3\mathrm{He})\rangle
\end{aligned}$$

$$+\left\{\frac{\sqrt{3}+1}{2}\overline{f}_{(\Sigma^+\pi^-)}+\frac{1}{2}\overline{f}_{(\Sigma^0\pi^-)}\right\}\langle\Psi^{1,1}_{(-)}|\Psi(^3\mathrm{He})\rangle$$
$$+\left\{\frac{\sqrt{3}-1}{2}\overline{f}_{(\Sigma^+\pi^-)}-\frac{1}{2}\overline{f}_{(\Sigma^0\pi^-)}\right\}\langle\Psi^{1,1}_{(+)}|\Psi(^3\mathrm{He})\rangle. \quad \text{(B3)}$$

We find that interference effects between $\overline{f}_{(\Sigma^+\pi^-)}$ and $\overline{f}_{(\Sigma^0\pi^-)}$ play an important role in populating $\Psi^{1,1}_{(-)}$ and $\Psi^{1,1}_{(+)}$ within the ΣNN states with $T=1$. Considering the relative phase $\varphi(\Sigma^+/\Sigma^0)=+4.8^\circ$ between $\overline{f}_{(\Sigma^+\pi^-)}$ and $\overline{f}_{(\Sigma^0\pi^-)}$ at $p_{K^-}=600$ MeV/c, we obtain that the component of $\Psi^{1,1}_{(-)}$ that is identified as the $^3_\Sigma$He quasibound state with $J^\pi=1/2^+$, $T=1$, is relatively enhanced in the π^- spectrum, whereas the component of $\Psi^{1,1}_{(+)}$ in Σ continuum states is reduced.

For the π^+ spectrum, we find that the $^3_\Sigma n$ quasibound state is populated via only $\overline{f}_{(\Sigma^-\pi^+)}$. We obtain

$$\Psi^{2,-1}_{(s)}=\frac{1}{\sqrt{2}}|\{pn\}\Sigma^-\rangle+\frac{1}{\sqrt{2}}|\{nn\}\Sigma^0\rangle,$$
$$\Psi^{1,-1}_{(s)}=\frac{1}{\sqrt{2}}|\{pn\}\Sigma^-\rangle-\frac{1}{\sqrt{2}}|\{nn\}\Sigma^0\rangle, \quad \text{(B4)}$$
$$\Psi^{1,-1}_{(t)}=|[pn]\Sigma^-\rangle,$$

where the isospin $T=1$ good states are written as

$$\Psi^{1,-1}_{(\pm)}=a\Psi^{1,-1}_{(s)}\pm b\Psi^{1,-1}_{(t)}. \quad \text{(B5)}$$

If $a=b=1/\sqrt{2}$, $\Psi^{1,-1}_{(-)}$ and $\Psi^{1,-1}_{(+)}$ are regarded as ground and excited states in $^3_\Sigma n$, respectively. Thus the production amplitude for the (K^-,π^+) reaction is

$$\langle^3_\Sigma n\,\pi^+|T|^3\mathrm{He}K^-\rangle$$
$$\simeq\overline{f}_{(\Sigma^-\pi^+)}\left\{\frac{1}{2}\langle\Psi^{2,-1}_{(s)}|\Psi(^3\mathrm{He})\rangle+\frac{2\sqrt{3}-\sqrt{2}}{4}\langle\Psi^{1,-1}_{(-)}|\Psi(^3\mathrm{He})\rangle+\frac{2\sqrt{3}+\sqrt{2}}{4}\langle\Psi^{1,-1}_{(+)}|\Psi(^3\mathrm{He})\rangle\right\}. \quad \text{(B6)}$$

We find that production amplitude for $\Psi^{1,-1}_{(-)}$ is relatively reduced by a factor $(2\sqrt{3}-\sqrt{2})/4=0.51$, whereas that for $\Psi^{1,-1}_{(+)}$ is enhanced by a factor $(2\sqrt{3}+\sqrt{2})/4=1.22$. This mechanism is inevitable whenever we consider the ^{3}He(K^-,π^+) reaction.

[1] E. Friedman and A. Gal, Phys. Rep. **452**, 89 (2007), and references therein.
[2] Y. Akaishi, T. Harada, S. Shinmura, and Khin Swe Myint, Phys. Rev. Lett. **84**, 3539 (2000), and references therein.
[3] For example, S. Balberg and A. Gal, Nucl. Phys. A **625**, 435 (1997); M. Baldo, G. F. Burgio, and H. J. Schulze, Phys. Rev. C **61**, 055801 (2000); S. Weissenbord *et al.*, Nucl. Phys. A **881**, 62 (2012).
[4] H. Tamura, Study of Σ-*N* interaction using light Σ-nuclear systems, Letter of Intent for J-PARC (2008), http://j-parc.jp/NuclPart/Proposal_e.html.
[5] C. B. Dover, D. J. Millener, and A. Gal, Phys. Rep. **184**, 1 (1989).
[6] R. E. Chrien, Proceedings of APCTP Workshop on Strangeness in Nuclear Physics (SNP 99), 19–22 Feb. 1999, Seoul, Korea, pp. 127-135.
[7] S. Bart *et al.*, Phys. Rev. Lett. **83**, 5238 (1999).
[8] R. S. Hayano *et al.*, Phys. Lett. B **231**, 355 (1989).
[9] H. Outa, T. Yamazaki, M. Iwasaki, and R. S. Hayano, Prog. Theor. Phys. Suppl. **117**, 171 (1994).
[10] T. Nagae *et al.*, Phys. Rev. Lett. **80**, 1605 (1998).
[11] T. Harada *et al.*, Nucl. Phys. A **507**, 715 (1990).
[12] P. K. Saha *et al.*, Phys. Rev. C **70**, 044613 (2004).
[13] M. Oka *et al.*, Phys. Lett. B **130**, 365 (1983).
[14] H. Garcilazo, J. Phys. G **13**, L63 (1987).
[15] A. Stadler and B. F. Gibson, Phys. Rev. C **50**, 512 (1994).
[16] I. R. Afnan and B. F. Gibson, Phys. Rev. C **47**, 1000 (1993).
[17] C. B. Dover, A. Gal, and D. J. Millener, Phys. Lett. B **138**, 337 (1984).
[18] Y. H. Koike and T. Harada, Nucl. Phys. A **611**, 461 (1996).
[19] H. Garcilazo, T. Fernández-Caramés, and A. Valcarce, Phys. Rev. C **75**, 034002 (2007).
[20] M. Barakat and E. V. Hungerford, Nucl. Phys. A **547**, 157c (1992).
[21] T. Harada and Y. Hirabayashi, Few-Body Syst. **54**, 1205 (2013).
[22] S. Shinmura (private communication) (2011).
[23] M. M. Nagels, T. A. Rijken, and J. J. de Swart, Phys. Rev. D **20**, 1633 (1979).
[24] R. H. Dalitz, R. C. Herndon, and Y. C. Tang, Nucl. Phys. B **47**, 109 (1972).
[25] H. Nemura, Y. Akaishi, and Y. Suzuki, AIP Conf. Proc. **644**, 56 (2002).
[26] M. M. Nagels, Th. A. Rijken, and J. J. de Swart, Phys. Rev. D **15**, 2547 (1977).
[27] H. Nemura, S. Shinmura, Y. Akaishi, and Khin Swe Myint, Phys. Rev. Lett. **94**, 202502 (2005); Nucl. Phys. A **754**, 110c (2005).
[28] O. Morimatsu and K. Yazaki, Nucl. Phys. A **435**, 727 (1985); **483**, 493 (1988).
[29] O. Morimatsu and K. Yazaki, Prog. Part. Nucl. Phys. **33**, 679 (1994).
[30] T. Harada, Phys. Rev. Lett. **81**, 5287 (1998).
[31] T. Harada, Nucl. Phys. A **672**, 181 (2000).
[32] Y. Akaishi, *International Review of Nuclear Physics 4* (World Scientific, Singapore, 1986), p. 259.
[33] H. Morita, Y. Akaishi, O. Endo, and H. Tanaka, Prog. Theor. Phys. **78**, 1117 (1987).
[34] M. Kamimura *et al.*, Prog. Theor. Phys. Suppl. **89**, 1 (1986).
[35] J. Hüfner, S. Y. Lee, and H. A. Weidenmüller, Nucl. Phys. A **234**, 429 (1974).
[36] A. Bouyssy, Nucl. Phys. A **290**, 324 (1977).
[37] E. H. Auerbach *et al.*, Ann. Phys. (NY) **148**, 381 (1983).
[38] S. Tadokoro, H. Kobayashi, and Y. Akaishi, Phys. Rev. C **51**, 2656 (1995).
[39] T. Koike and T. Harada, Nucl. Phys. A **804**, 231 (2008).

[40] C. B. Dover and A. Gal, Ann. Phys. (NY) **146**, 309 (1983).
[41] T. Harada and Y. Hirabayashi, Nucl. Phys. A **744**, 323 (2004).
[42] C. B. Dover, L. Ludeking, and G. E. Walker, Phys. Rev. C **22**, 2073 (1980).
[43] See, e.g., R. G. Newton, *Scattering Theory of Waves and Particles*, 2nd ed. (Springer-Verlag, New York, 1982).
[44] T. Harada and Y. Akaishi, Prog. Theor. Phys. **96**, 145 (1996).
[45] T. Udagawa, P. Oltmanns, F. Osterfeld, and S. W. Hong, Phys. Rev. C **49**, 3162 (1994).
[46] A. S. Rosenthal and F. Tabakin, Phys. Rev. C **22**, 711 (1980).
[47] B. W. Allardyce *et al.*, Nucl. Phys. A **209**, 1 (1973).
[48] C. B. Dover and G. E. Walker, Phys. Rev. C **19**, 1393 (1979); Phys. Rep. **89**, 1 (1982).
[49] G. P. Gopal *et al.*, Nucl. Phys. B **119**, 362 (1977).
[50] J. Dabrowski, Phys. Rev. C **8**, 835 (1973).
[51] H. Bandō and S. Nagata, Prog. Theor. Phys. **67**, 1312 (1982); Y. Yamamoto and H. Bandō, Prog. Theor. Phys. Suppl. **81**, 9 (1985).
[52] J. P. Jeukenne, A. Lejeune, and C. Mahaux, Phys. Rev. C **16**, 80 (1977).
[53] Th. A. Rijken *et al.*, Prog. Theor. Phys. Suppl. **185**, 14 (2010); Y. Fujiwara *et al.*, Prog. Part. Nucl. Phys. **58**, 439 (2007); H. Polinder *et al.*, Phys. Lett. B **653**, 29 (2007); T. Inoue *et al.*, Phys. Rev. Lett. **106**, 162002 (2011).
[54] A. T. Kruppa, R. G. Lovas, and B. Gyarmati, Phys. Rev. C **37**, 383 (1988).
[55] S. Aoyama, T. Myo, K. Katō, and K. Ikeda, Prog. Theor. Phys. **116**, 1 (2006).
[56] M. Jurič *et al.*, Nucl. Phys. B **52**, 1 (1973).
[57] J. Dabrowski and M. Y. M. Hassan, Phys. Rev. C **1**, 1883 (1970).
[58] H. Bandō and I. Shimodaya, Prog. Theor. Phys. **63**, 1812 (1980).